VOLUME 1, No. 7 (1956)

NUCLEAR PHYSICS

MONTHLY JOURNAL DEVOTED TO THE EXPERIMENTAL AND THEORETICAL STUDY OF ATOMIC NUCLEI, NUCLEAR FIELDS AND THE FUNDAMENTAL ASPECTS OF COSMIC RADIATION

EDITOR: L. ROSENFELD - MANCHESTER

E. Schalscha, Radioactive decay of ruthenium-95 481

S. K. Bhattacherjee and Shree Raman, Decay of Gd^{153}. . 486

R. Nordhagen and J. Thomassen, γ-Rays from the decay of Zr^{97} 499

G. Bozóki, E. Fenyves and L. Jánossy, On the penetrating non-ionizing component of cosmic rays 501

M. Demeur, On the anomalous L-X-ray yield in light mesic atoms 516

Colloque de physique nucléaire 530

Book reviews 537

Symbols and Units 539

NORTH-HOLLAND PUBLISHING COMPANY - AMSTERDAM

June 1956

EDITORIAL BOARD

AUSTRIA:	B. Karlik (Vienna), H. Thirring (Vienna)
BELGIUM:	M. de Hemptinne (Louvain), J. Verhaeghe (Ghent)
CANADA:	G. Volkoff (Vancouver)
DENMARK:	C. Møller (Copenhagen), S. Rozental (Copenhagen)
EGYPT & ARAB COUNTRIES:	F. El Bedewi (Alexandria), M. G. Nooh (Cairo)
FINLAND:	L. Simons (Helsinki)
FRANCE:	A. Berthelot (Saclay), S. Gorodetzky (Strasbourg), F. Joliot (Paris)
GERMANY:	W. Gentner (Freiburg i. B.), J. H. D. Jensen (Heidelberg)
GREAT BRITAIN:	S. Devons (Manchester)
HUNGARY:	L. Janossy (Budapest)
INDIA:	H. Bhabha (Bombay), B. Peters (Bombay), R. Ramanna (Trombay)
IRISH REPUBLIC:	J. McConnell (Maynooth)
ISRAEL:	G. Racah (Jerusalem)
ITALY:	E. Amaldi (Rome)
JAPAN:	S. Kikuchi (Tokyo), S. Tomonaga (Tokyo)
NETHERLANDS:	H. Brinkman (Groningen), S. R. de Groot (Leiden)
NORWAY:	E. Hylleraas (Oslo), A. Lundby (Oslo), H. Wergeland (Trondheim)
POLAND:	L. Infeld (Warsaw)
PORTUGAL:	J. M. Araújo (Porto), J. R. de Almeida Santos (Coimbra)
SOUTH AMERICA:	G. Beck (Saõ Paulo), J. Leite Lopes (Rio de Janeiro)
SPAIN:	J. M. Otero (Madrid), C. Sanchez del Rio (Madrid)
SWEDEN:	O. Klein (Stockholm), K. Siegbahn (Uppsala), I. Waller (Uppsala)
SWITZERLAND:	P. Huber (Basel), P. Scherrer (Zürich)
U.S.S.R.:	M. A. Markov (Moscow), I. S. Shapiro (Moscow), D. V. Skobeltzyn (Moscow)
YUGOSLAVIA:	I. Supek (Zagreb)
U.S.A. & MEXICO:	V. Weisskopf (Cambridge, Mass.)
AUSTRALIA & NEW ZEALAND:	H. Messel (Sydney), M. L. Oliphant (Canberra)

CONTRIBUTIONS may be sent to the Editor, Professor L. Rosenfeld, Dept. of Theoretical Physics, The University, Manchester, either directly, or preferably through the intermediary of one of the members of the Editorial Board of the country or region in which the author is working. They may be written in English, French or German.

BOOKS FOR REVIEW should be sent to Professor Rosenfeld.

NUCLEAR PHYSICS is published in monthly issues. The subscription price of a volume of 700 pages is fl 57.00; 114s; $ 15.00. Postfree.

SUBSCRIPTIONS should be sent to the publishers, NORTH-HOLLAND PUBLISHING COMPANY, P.O.Box 103, Amsterdam or to any subscription-agent. Subscriptions for U.S.A. are to be sent exclusively to INTERSCIENCE PUBLISHERS, INC., 250 Fifth Avenue, New York 1, N.Y.

Printed in the Netherlands.

Nuclear Physics, North-Holland Publishing Co., Amsterdam, **1**, (**1956**)

RADIOACTIVE DECAY OF RUTHENIUM-95

EDUARDO SCHALSCHA B.Q.F.

Instituut voor Kernphysisch Onderzoek, Amsterdam †

Received 27 February 1956

Abstract: Ruthenium 95, produced by a (n,2n) reaction, was studied by scintillation spectrometry, and the half-life and positon energy were determined by magnetic deflector and absorption measurements in Geiger-Müller beta counters.

The isotope decays with a half-life of 1.65 ± 0.05 h by emission of positons with a maximum energy of 1.2 ± 0.1 MeV and by electron capture combined with emission of γ-rays of 145, 340, 640 and 1110 keV.

Nuclear level schemes are discussed.

1. Experimental

Ru^{95} was discovered by Eggen and Pool[1]) who prepared it by means of the reaction $Mo^{92}(\alpha,n)Ru^{95}$. We were unable to study Ru^{95} in preparations obtained by α-irradiation of molybdenum in the Philips' Cyclotron, as the higher α-energy gives rise [2]) to the formation of a strong activity of Ru^{94}, the Tc^{94} daughter of which obscures the observation of Ru^{95}. For this reason we made use of the process $Ru^{96}(n,2n)Ru^{95}$.

In the present investigation ruthenium metal powder was irradiated for periods of one hour with fast neutrons from the bombardment of beryllium with 26 MeV deuterons in the Philips' Cyclotron.

Following a chemical purification of the irradiated material radioactive sources were studied with Geiger-Müller counters both with and without a magnetic deflector for separation of positons and negatons.

The purification was accomplished by boiling the irradiated metal in 4N sodium hydroxide and potassium persulfate until the sample was completely dissolved. Potassium permanganate solution, water and concentrated sulfuric acid were then added, and RuO_4

† Present address: Laboratorio de Fisica Nuclear de la Universidad de Chile, Santiago de Chile.

was distilled and collected in 4N sodium hydroxide. This solution was then treated with 96 % ethanol to precipitate the ruthenium as a hydrated oxide of ruthenium, centrifuged, filtered and dried. The whole chemical operation takes about 20 to 25 minutes.

The analysis of the beta decay scheme showed the presence of 100 min, 4.5 h and 2.6 d activities.

The half-life of the positon activity was determined by means of a counter with magnetic deflector and found to be 1.65 ± 0.05 h, exactly as was reported by Eggen and Pool [1]).

The maximum energy of the positons was determined by Feather analysis of an isochronous aluminium absorption curve. Decay curves were obtained through eight different absorbers. Each decay curve was analyzed to give the three periods indicated above and the activity of the 100 min component at one selected time was used for Feather analysis relative to a N^{13} standard ($E_{\beta+} = 1.25$ MeV). From the range-energy relation plot [3]) the maximum beta energy was found to be 1.2 ± 0.1 MeV which is in excellent agreement with previously reported data [1]).

The γ-spectrum was analyzed in a sliding channel scintillation spectrometer with a NaI(T1) crystal. The efficiency curve of the instrument was obtained using Au^{198}, Hg^{203}, Cs^{137}, Bi^{206} and Na^{22}. The energies of the γ-lines were obtained by comparison with the 661 keV line of Cs^{137} and the 122.8 line of Co^{57}.

In table I the energies of the γ-lines are given as well as their intensities relative to β^+ (given by one half of the 0.51 MeV peak intensity).

TABLE I

γ-ray spectrum of Ru^{95}

Energy in keV	Intensity Ratio γ/β^+
1110 ± 20	1.0
640 ± 8	0.5
511	
340 ± 8	4.0
≈ 145	≈ 1

From these data it may be concluded that there are at least four γ-rays due to the Ru^{95} decay with energies of 145, 340, 640 and 1110 keV. The photopeaks of these γ-rays decay with the right half-life, the same as the annihilation peak. The 145 keV level is uncertain and may be due to more than one γ-ray.

2. Discussion

From the experimental results obtained we can conclude that much of the decay goes primarily to the 340 keV level.

Using the tables and graphs of Zweifel [4]) and of Feenberg [5]) the ratio of electron capture to positon emission for an allowed transition was calculated and found to be E.C./$\beta^+ \approx 2$.

The log *ft* value calculated for the β^+-process according to Moszkowski [6]) was found to be 5 which indicates an allowed β-process.

It would be tempting to assume a decay-scheme for Ru^{95} similar to that proposed for Ru^{97} by Cork *et al.* [7]). There can be little doubt that in Tc^{95} the 20-hour period represents the ground state ($g_{9/2}$) and the 60-day period the $p_{1/2}$-isomer. If it is assumed that the ground state of Ru^{95} is $d_{5/2}$ as it is in Ru^{97} and that there is an 0.38 MeV $p_{3/2}$ state in Tc^{95}, nearly all β^+-transitions and the main electron capture decay of Ru^{95} would be to this level which should go to the 0.04 MeV excited state in Tc^{95}. Another E.C. branch would go to a 1.165 MeV state of Tc^{95}, which would decay partly to the ground state by single γ-ray emission, partly to the excited state via a cascade of three γ-rays of which the 0.340 MeV line would be the third. However, according to this scheme, the decay to the 0.38 MeV state should be first-forbidden because of a change of parity, and the *ft*-value, which is found to be around 10^5, makes this assumption seem rather unlikely.

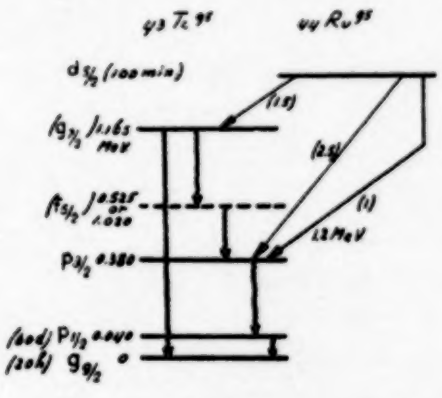

Fig. 1

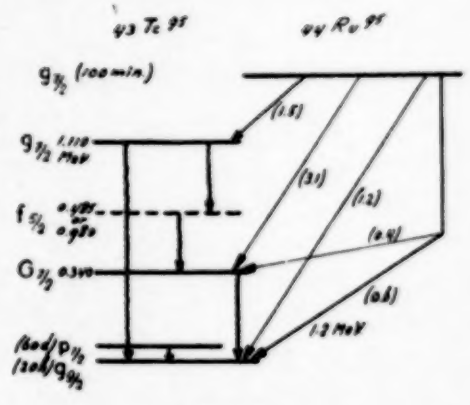

Fig. 2

Figure 1. First suggested decay scheme for Ru^{95}. The value of 1.165 MeV for the highest level in Tc^{95} is obtained by adding the energies of the γ-lines in the cascade. It does not agree well with the value 1.110 MeV determined by direct measurement.

Figure 2. Second suggested decay scheme for Ru^{95}. The value of 1.110 MeV for the highest level in Tc^{95} is determined by direct measurement. It is in fair agreement with the figure 1.125 MeV obtained by adding the energies of the γ-lines in the cascade.

Dr Wapstra has suggested an alternative scheme to us, in which the ground state of Ru^{95} is a $g_{7/2}$ level and in which the 0.34 level in Tc^{95} is a $G_{7/2}$ combination state. In this case the β^--transition is mainly to the ground state of Tc^{95} but for a smaller fraction to the 0.34 MeV-level. The ground state and the levels at 0.34 MeV and at 1.110 MeV are all fed by electron-capture.

In figure 1 and in figure 2 the two discussed decay schemes are given. The γ-energies are in better agreement with the second scheme than with the first.

The uncertainty of the intensity of the 0.145 MeV line makes it impossible to decide whether it is fed only by the 0.640 MeV γ-transition or whether it is fed partly or entirely by electron capture. Under these circumstances we are unable to indicate the sequence of the 0.145 MeV and the 0.640 MeV γ-ray transition, but, of course, there cannot be any doubt that the 0.340 MeV γ-ray leads directly to the ground state or to the isomeric state.

3. Theoretical Considerations

Of the decay schemes discussed by us the first one leads to a total decay energy of 2.6 MeV for Ru^{95}, and the second one gives a decay energy of 2.2 MeV. It is a matter of some interest to compare these figures to a calculated value. The latter we have obtained by applying to the decay-energy, calculated for the liquid drop model by C. N. Martin [8]), an empirical correction which we have determined from the difference between the observed and the theoretical value of the decay-energy of Y^{91}. This choice was made because our transition takes place near the magic neutron number 50, and the number of neutrons in Ru^{95} and in Tc^{95} is equal to that in Zr^{91} and Y^{91}. In this way we calculated a decay-energy of 3.0 MeV for Ru^{95}, which is in reasonable agreement with our first decay-scheme.

This work is part of the programme of the Foundation for Fundamental Research of Matter (F.O.M.) which is carried out with the support of the Netherlands Organization for Pure Research (Z.W.O.) The author wishes to extend special thanks to Professor Dr A. H. W. Aten Junior for his help and guidance in this work and to Dr A. H. Wapstra for helping to interpret the experimental facts.

To the chemical department of the Instituut voor Kernphysisch Onderzoek and to Philips' Cyclotron personnel my thanks are due for their help and collaboration. The author could carry out this

work in the Netherlands due to a grant obtained from the Rector of the Universidad de Chile, Professor Dr Gomez Millas, to whom he wants to express his gratitude on this occasion.

References

1) D. T. Eggen and M. L. Pool, Phys. Rev. **74** (1948) 57
2) A. v. d. Wiel and A. H. W. Aten Junior, Physica **18** (1952) 356
3) L. G. Glendenin, Nucleonics **2** (1948) 16
4) P. F. Zweifel, Phys. Rev. **96** (1954) 1572
5) E. Feenberg and G. Trigg, Rev. Mod. Phys. **22** (1950) 388
6) S. A. Moszkowski, Phys. Rev. **82** (1951) 35
7) M. L. Cook, M. K. Brice, L. C. Schmid and R. G. Helmer, Phys. Rev. **100** (1955) 188
8) C. N. Martin, Numerical Tables of Nuclear Physics (Gauthier-Villars, Paris 1954)

Nuclear Physics, North-Holland Publishing Co., Amsterdam, **1**, **(1956)**

DECAY OF Gd^{153}

S. K. BHATTACHERJEE and SHREE RAMAN

Tata Institute of Fundamental Research, Bombay

Received 8 March 1956

Abstract: The decay by electron capture of Gd^{153} (half-life 236 days) is studied with a coincidence Scintillation Spectrometer. Two gamma-rays are observed with energies 72 ± 8 keV and 100 ± 4 keV and relative intensities of 7 : 100. Both these gamma-rays are coincident with K X-rays of Eu. From the coincidence data the K-shell conversion coefficient of the 100 keV gamma transition has been determined to be 0.67 ± 0.12; the comparison with theory then leads to assigning this gamma-ray predominantly to a magnetic dipole transition. From the experimental L/K capture ratio the energy involved in the capture process is estimated. Our results show that the levels in Eu^{153} which are reached by the capture decay of Gd^{153} are not identical with the levels that were observed in coulomb excitation of Eu. On the basis of our findings we propose a decay scheme for Gd^{153}.

1. Introduction

By deuteron bombardment of purified europium Fajans and Voigt [1]) first observed an activity of a half life of 155 to 170 days which was assigned to Gd^{153}. A 236 day neutron induced activity [2]) in gadolinium indicated only one gamma-ray with an energy of 106 keV. The presence of L X-rays and L-conversion electrons was inferred from aluminium absorption curves by Hein and Voigt [2]). Cork [3]) and his co-workers studied the conversion electron spectrum of Gd^{153} in a high resolution magnetic spectrometer. Only one gamma-ray corresponding to an energy of 103.7 keV with a K/L conversion ratio of 5.2 ± 1 was reported by them. McGowan[4]) reports that the 102 keV in Eu^{153} reached by electron capture disintegration of Gd^{153} decays with $T_{\frac{1}{2}} = 3.4 \times 10^{-9}$ sec; he also reports the existence of another equally abundant level very close to this, which is in prompt coincidence with the K X-rays. The levels of Eu^{153} are also reached by the beta-decay[5–11]) of 47 hour Sm^{153}. In an analysis of β-spectra, Lee and Katz [7]) find three β^--groups with maximum energies of 0.255, 0.685 and 0.795 MeV with relative intensities of 9, 70 and 21 percent respectively, the 0.795 MeV group going directly

to the ground state of Eu^{153}. In the electron-spectrum they observed three gamma-rays at 69, 102 and a very weak one at 548 keV. Most of the workers[5–11]) are in good agreement as to the value of K/L to be 6.2 for the most prominent gamma-ray of 102 keV; however, Siegbahn[5]) and Lee and Katz[7]) report for the K-conversion coefficient α_K for 102 keV gamma-ray the value of about 0.6 whereas Sunyar [8]), McGowan [4]) and Marty [11]) report about 1.2.

Recently, three gamma-rays at 82, 102 and 187 keV have been observed by Heydenburg and Temmer [12]) and by Mark and Paulissen [13]) in the coulomb excitation of europium by bombarding natural Eu_2O_2 with alpha-particles and protons. Heydenburg and Temmer have also shown that some of the 82 keV radiation is in cascade with the 102 keV gamma-ray, representing a well-developed rotational spectrum.

The present work was undertaken in order to study the levels in Eu^{153} reached by electron-capture decay of 236-d Gd^{153} by a Single Crystal NaI (Tl) Spectrometer and a Coincidence Scintillation Spectrometer. We investigated the gamma-spectrum: the existence of weak lines was established by absorption technique; we found α_K for 102 keV gamma-ray by coincidence technique [14]) and thus determined the multipole character of this transition. Our results give the ratio of L/K capture and the electron capture decay energy was estimated from Marshak's formula; from the corresponding log *ft*-value the order of transition was classified. A decay scheme for Gd^{153} is proposed.

2. Experimental Procedure

For gamma detection, scintillation detectors consisting ot thalium-activated sodium iodide crystals were used. One photomultiplier head consists of a Dumont 6292 photo tube with a NaI (Tl) crystal of $1\frac{3}{4}''$ diameter and 1″ thick (Harshaw Chemicals) optically coupled to it by Silicone grease. The other spectrometer head has one RCA 5819 tube with $1\frac{3}{4}''$ diameter $\frac{1}{2}''$ thick NaI (Tl) crystal optically mounted to the photocathode through a perspex light guide. We call the 1″ thick (6292 tube) crystal "master" crystal and the $\frac{1}{2}''$ thick the "gate" crystal (5819 tube). In coincidence spectrometer all gamma-energies and intensities are measured in the master crystal spectrometer. In most of the experiments the two photomultiplier heads were oriented at 180° with repect to each other, one on top of the other with the source in between. Both

the photomultipliers and the two associated crystals were shielded by 1½" thick lead to minimise background interferences. In our coincidence experiment the two photomultiplier detector heads were oriented at 90° with respect to each other with a shield in between avoid iodine K X-rays escaping from one detector into the other thus giving false coincidences in the low energy region. The coincidence scintillation spectrometer usually employs the 'fast-slow method' with about 10^{-7} sec as the resolving time for the fast-coincidence portion. In order to reduce considerably the time of observation where particularly fast coincidence is not a necessity one can bypass the time discriminator part of the instrument. In this work a resolving time of about 2.5×10^{-7} sec was maintained throughout. Each single channel spectrometer consists of a non-overloading [15]) linear amplifier the input of which is fed by the positive pulse from the tenth dynode of each photomultiplier. The amplifier output pulses are analysed by single channel analysers as designed by Johnstone [19]) employing 6BN6 gated-beam tubes. The outputs of these two analysers were fed directly to the coincidence circuit which consists of univibrators as pulse shapers. The mixer tube employed is 6F33. Appropriate delays were inserted in order to compensate for different times of travel of the coincident pulses in the two channels of the spectrometer. In this way only those coincidences were selected corresponding to signals from the master crystal and gate crystal whose amplitudes after appropriate amplifications fall within the respective windows of the analysers.

The master spectrometer was calibrated with the following known gamma-rays: 53 keV Yb K X-rays and 84 keV gamma-ray of Tm^{170}, the 70 keV Hg K X-ray and 411 keV gamma-ray of Au^{198}, 311 keV gamma-ray of Cr^{51}, 510 keV annihilation radiation of Na^{22} and 661 keV Cs ^{137} gamma-ray. The photopeak width at half-maximum for 661 keV Cs^{137} gamma-ray was about 8 %. From the measured ratios of photopeak to total area in the scintillation spectra of the mono-energic sources like 84 keV Tm^{170} gamma-ray, 331 keV in Cr^{51}, 411 keV in Au^{198}, 661 keV in Cs^{137}, 510 keV annihilation radiation and 1.28 MeV gamma-ray in Na^{22}, 1.1 MeV in Zn^{65} and from the dimension of the crystal as well as from the known detection geometry an usuful efficiency curve [17]) was obtained for our master crystal. It may be noted that the source to crystal distance in all the experiments reported here was kept rather large in order to keep the contribution of degraded gamma radiation by the surroun-

dings to a minimum; also the pile-up effect of coincident gamma-rays was avoided. In almost all cases the scanning window in the master spectrometer was 1 Volt whereas the window of the gate spectrometer was allowed to accept the full-energy pulse spectrum peak of the gamma or X-ray as the case may be.

3. Energies and Relative Intensities of the Gamma Rays

The pulse-height distribution generated in the master crystal by the gamma-rays following electron capture decay of Gd^{153} is shown in Fig. 1 and Fig. 2. From these scintillation spectra it is clear

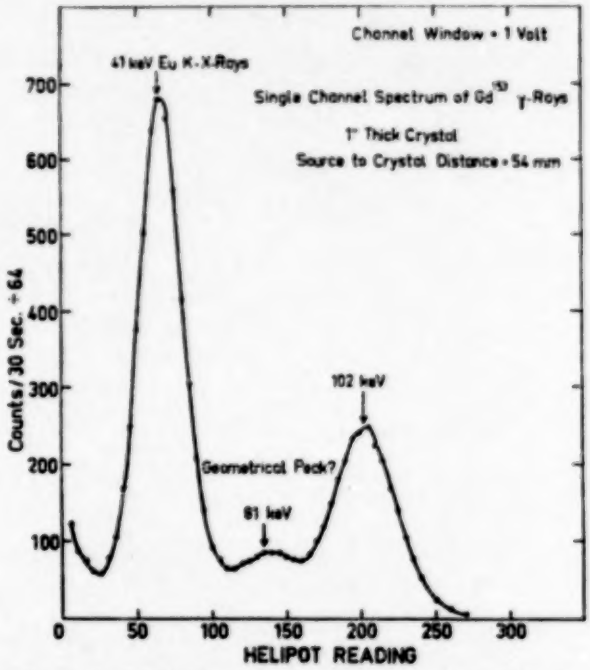

Figure 1. Single Crystal Spectrum of Gd^{153}. The intensity of the broad hump at ≈ 81 keV peak cannot be explained alone by the iodine K X-ray escape of 102 keV gamma-ray. Scanning window is 1 volt.

that the quantum radiations of Gd^{153} consist of an intense peak corresponding to 41 keV X-rays of Eu and a strong gamma-ray of 100 ± 4 keV energy. In Fig. 1 one notices a weak but distinct peak at $\approx$ 80 keV. In order to check whether this is a build-up pulse due to simultaneous detection in the crystal of two K X-rays of Eu, the source to crystal distance was reduced from 54 mm to 19 mm and the experiment was repeated. Fig. 2 shows the result. One notices the intense X-ray peak, the strong 102 keV peak and a small peak at 146 keV; another weak peak is also observed corresponding to a gamma-ray of 305 keV. One fails to notice any peak at $\approx$ 80 keV here, which, if it were a built-up peak, must have appeared rather

prominently now, since the source to crystal distance is less. On the other hand the 146 keV peak appears now, which was not observed for a source to crystal distance of 54 mm (fig. 1). Hence the peak at 80 keV in Fig. 1 is probably a genuine peak due to a gamma-ray, the peak at 146 keV in Fig. 2 is a build-up peak and is presumably due to the simultaneous detection of an X-ray and 102 keV gamma ray.

In order to investigate further the nature of the origin of the 146 keV peak we put 160 mg/cm^2 of tin absorber between the source and the master crystal and we measured the whole spectrum at the same geometry. The results are shown as the dotted curve in Fig. 2.

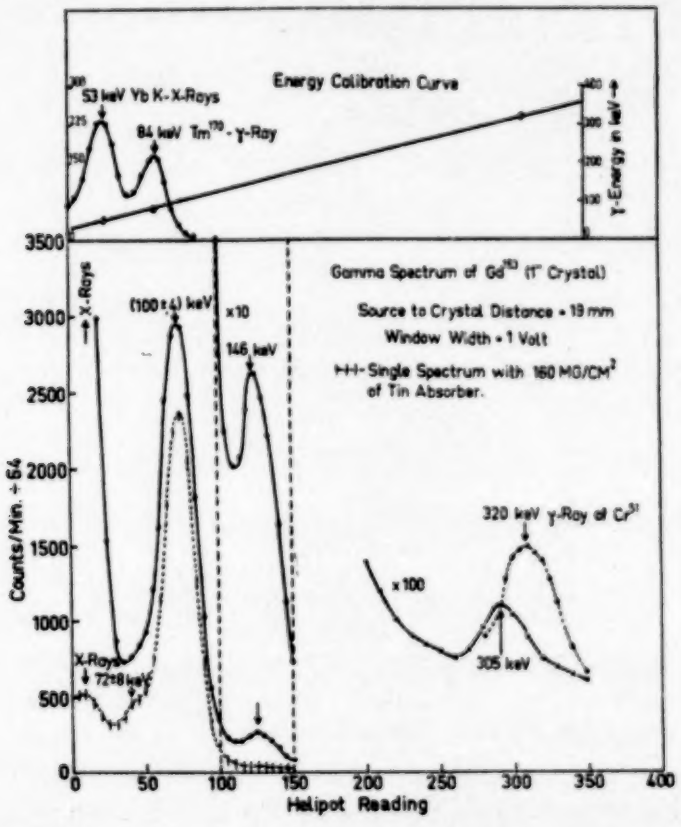

Figure 2. Single Crystal Spectrum of Gd^{153} with a different source to crystal distance. The dotted curve is taken with 160 mg/cm^2 of Sn absorber.

Here the 146 keV peak is washed out completely which proves that it is a buildup peak since it follows the absorption coefficient of a lower energy component in tin than it should, if it were due to radiations of 146 keV energy: consequently one concludes that it is a sum of one K X-ray and one 102 keV gamma-ray. It is also interesting to note that in the absorption spectrum there is distinct evidence of the presence of a gamma-ray of energy (72$\pm$8) keV.

The large error in determining the energy of this gamma-ray is due to the fact that the escape peak due to 102 keV gamma-ray falls in this region of the spectrum: the contribution of escape peak alone, however, cannot explain the observed intensity here. Eu K X-rays at 41 keV are absorbed in tin very rapidly as can be seen in the absorption spectrum; if the peak at 72 keV were a buildup of two X-rays then it would follow the absorption coefficient of radiations corresponding to an energy of 41 keV in tin and naturally the corresponding portion of the spectrum would have depressed much more than one can notice in the absorption spectrum. This absorption experiment clearly establishes the existence of a gamma-ray $\approx$ 72 keV in Gd^{153} electron capture decay though in weak intensity.

Higher energy gamma-rays were looked for but, besides the 305 keV one, no other gamma-ray was found. The 305 keV gamma-ray observed here may be identified with the one observed at 310 keV in the Coulomb excitation of natural Eu. They assigned this gamma-ray to Eu^{151} mainly because some evidence of a gamma-ray of 270 keV following the capture decay of 150d Gd^{153} is reported in the literature [18]). After making suitable correction [4, 19]) due to the escape peak contribution of 102 keV gamma-ray the relative intensities of the two gamma-rays of 72 keV and 102 keV were found to be 7 : 100.

4. Coincidence Measurements

With the gating channel set to accept the full photopeak of 41 keV Eu K X-rays, the coincidences which occurred as the master spectrometer scanned the entire spectrum are shown in Fig. 3. The scanning channel was swept over the whole region of interest. The X—X and X—γ coincidence peaks are expected if the decay of Gd^{153} occurs by K-electron capture to the levels in Eu^{153}, which decay by internally converted gamma-rays. The coincidence spectrum is shown by the dotted curve in Fig. 3 and 4, the calculated probable statistical errors are also shown. Because of the very weak intensity of the 72 keV gamma-ray one can conclude from the coincidence spectrum that there is some evidence of X—72 keV coincidences; the nature of 146 keV peak as a sum peak comprising of an X-ray and a gamma-ray is also established from the coincidence spectrum.

The whole spectrum was taken in the master crystal with the gating spectrometer accepting the full 102 keV gamma-ray peak. The results (not shown) show only one (X—γ) peak and no appreciable (γ—γ) coincidences.

Let N_{xx} represent the number of coincidences between X-rays, $N_{x\gamma}$ the number of coincidences between the X-rays and 102 keV

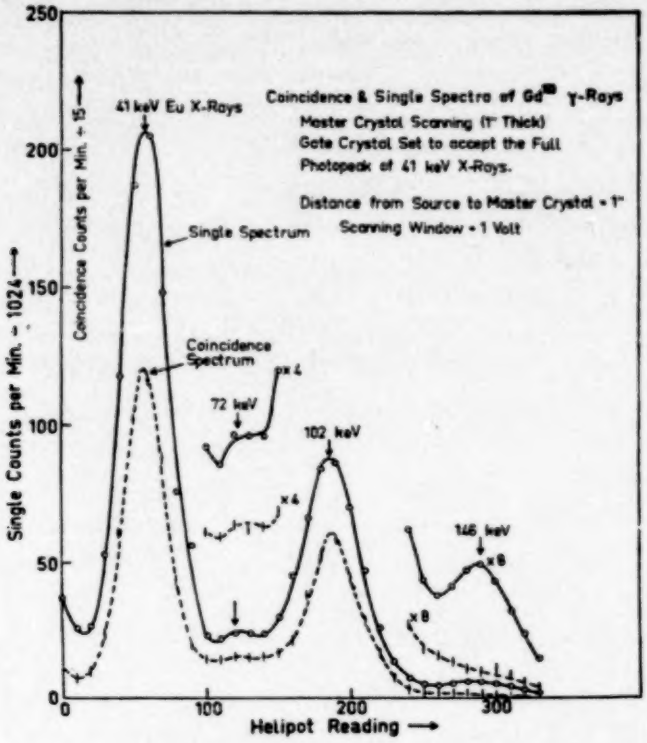
Coincidence & Single Spectra of Gd¹⁵³ γ-Rays
Master Crystal Scanning (1" Thick)
Gate Crystal Set to accept the Full
Photopeak of 41 keV X-Rays.
Distance from Source to Master Crystal = 1"
Scanning Window = 1 Volt
41 keV Eu X-Rays
Single Spectrum
Coincidence Spectrum
72 keV
102 keV
146 keV
Coincidence Counts per Min. ÷ 15
Single Counts per Min. ÷ 1024
Helipot Reading

Figure 3. The singles and coincidence spectra. The coincidence spectrum was taken in the master crystal with the gate crystal accepting the full photopeak of 41 keV Eu X-rays. The axes of the two counter-heads are at 180°.

gamma-rays, N_x number of single counts due to X-rays and N_γ the number of single counts due to 102 keV gamma-ray recorded in the master crystal while measuring N_{xx} and $N_{x\gamma}$. Then let us define, after Pruett and Wilkinson [14],

$$R_\theta = \frac{N_{x\gamma}}{N_\gamma} \Big/ \frac{N_{xx}}{N_x}.$$

In order to avoid the error introduced due to variation of efficiency with energy the quantity R_θ was obtained, at a number of corresponding points on the curves near the peaks after normalizing the coincidence curve to the singles curve at the gamma peak. The mean value of R_θ at three points close to peaks is 1.28 ± 0.08. The correction due to coincidences in the neighbourhood of the X-ray peak due to the Compton distribution of the gamma-ray is neglected

in view of the fact that the 102 keV gamma-ray suffers almost total absorption in the master crystal.

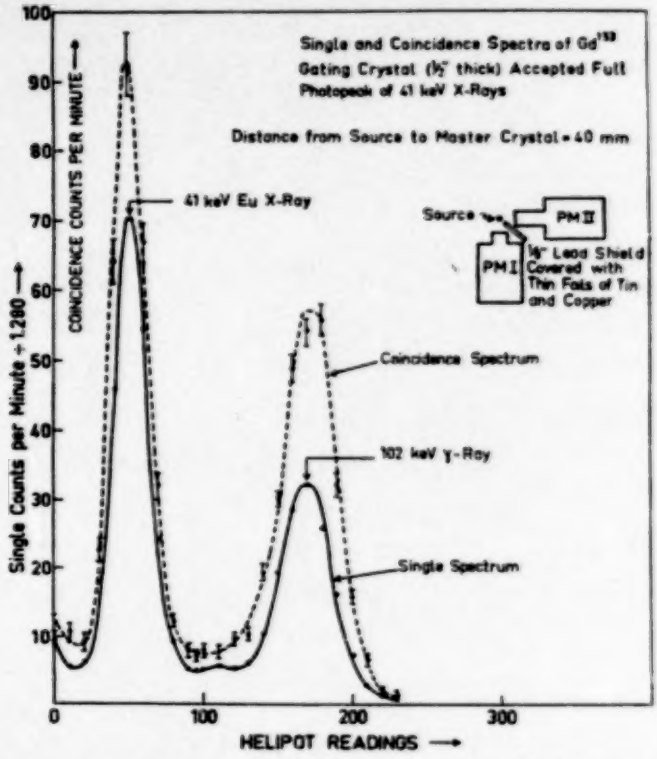

Figure 4. The singles and coincidence spectra with the counter-head axes oriented at 90°. A shield consisting of $\frac{1}{8}$″ thick Pb covered with 0.07″ thick Sn and 0.02″ Cu foils is used as shown at the inset.

Another experimentally determined quantity is the ratio, R_ϕ, of the number of K X-rays to the number of gamma-rays, N_{KX}/N_γ. R_ϕ is obtained from the measured areas under the X-ray and the gamma-ray photopeaks. The observed ratio has to be corrected for energy dependence of counter efficiencies, absorption in the crystal holder and the escape of iodine K X-rays for the X-ray as well as for the gamma-ray peaks. The escape peak correction was made from the experimental results of McGowan [4]), Mann [19]) *et al.* The correction factors were also confirmed by the theoretical calculation for good geometry case by Axel [20]). The corrected value of $R_\phi = 1.62 \pm 0.32$.

It has been shown [14]) that

$$N_K = (2R_\phi - 1)\alpha_K N_\gamma,$$

where N_K is the total number of K-captures and α_K is the K-shell conversion coefficient of 102 keV gamma-ray. Since the total number of K X-rays observed, N_{KX}, is equal to the sum of the total number of K-captures and total number of K-conversions, one gets immediately

$$N_{KX}/\omega_K = 2\, R_\theta \alpha_K N_\gamma,$$

where ω_K is the K-fluorescence yield, and hence,

$$\alpha_K = \frac{R_\phi}{2\omega_K R_\theta},$$

thus giving α_K directly in terms of the experimentally determined quantities R_θ and R_ϕ. The value α_K is found to be 0.67 ± 0.12, most of the error coming from the uncertainties in the correction for escape peak in R_ϕ.

5. Results and Discussions

From the table [22]) of theoretically calculated K-shell internal conversion coefficients we reproduce in Table I the relevant portion in order to compare the theoretical values with our α_K value and to assign the proper multipole order.

TABLE I.

Comparison of the theoretically calculated values of α_K in the regions of z close to 63 and for 102 keV energy with the experimentally observed value of $\alpha_K = 0.67 \pm 0.12$

Z	k_2 (mc units)	E1	E2	E3	M1	M2	M3	Remarks
64	0.3	0.079	0.345	1.28	0.575	3.44	16.13	Unscreened
55	0.2	0.173	1.11	5.88	0.760	6.70	45.2	Screened

From the above table one concludes that the 102 keV transition is predominantly of M1 type ($\triangle I = 1$, No.). This assignment is also supported if one inspects the extrapolated plot for $Z = 64$ of K-shell electric and magnetic conversion coefficients as given in Fig. 1, page 407 of ref. [22]) provided one extrapolates at $k = 0.2$.

The ratio of L-shell to K-shell captures to the excited state in Eu^{153} at 102 keV, ϵ, is given by the expression [14])

$$(2R_\theta - 1)(1+\epsilon)/(1+\beta) = (1+\alpha_T)/\alpha_K,$$

where β is the ratio of ground state to excited state K-shell capture.

Taking K/L = 6.2 and L/M = 4.5 as found by Marty [11]), $\alpha_T = 0.82$, one gets

$$\epsilon = 0.42 + 1.42\beta.$$

Although our experimental results do not give quantitatively the fraction of K-captures going to the ground state in Eu^{153}, still one can show from the intensities of K X-rays and 102 keV gamma-ray from the Single Channel Spectrum, and also from the fact that $\alpha_K = 0.67$ that the K X-rays arising due to K-captures going directly to ground state may be small. Thus, assuming $\beta \approx 0$, $\epsilon \approx 0.42$.

Marshak [23]) has shown that L-capture always accompanies K-captures and occurs with increasing probability as the transition energy becomes small and Z large. For allowed transitions

$$\epsilon = (\psi_{L_I}/\psi_K)^2 \left[\frac{w_0 + w_{L_I}}{w_0 + w_K}\right]^2$$

where w_0 is the decay energy.

From Rose and Jackson's [24]) curve, the value $(\psi_{L_I}/\psi_K)^2 = 0.133$ for $Z = 63$. From current values of electron binding energies [25]) one gets w_K and w_{L_I}, for Eu as 48.5 and 8 keV respectively. If $w_0 > w_K$ then one finds $\epsilon \approx 0.133$ i.e., the experimentally determined ratio of L to K capture is about three times the theoretical value. Thus one concludes that the decay energy w_0 to the excited state is not very large and hence the magnitude of w_K cannot be neglected in comparison to w_0. Assuming an allowed transition one gets $w_0 = 98$ keV as the transition energy for the electron capture decay of Gd^{153} to the excited state of Eu^{153} at 102 keV. The corresponding comparative half-life, log ft-value, is about 5.8 as obtained from the nomograph of Moszkowski [26]).

The value of L/K capture ratio of ≈ 0.42 and decay energy of ≈ 100 keV to the excited state of Eu^{153} ($Z = 63$) can be compared with some of the existing data in high Z electron capturing nucleides as reviewed by Robinson and Fink [27]). Recently from this Institute Gupta and Jha [28]) have determined the total decay energy of Gd^{153} electron capture decay by the crystal summing technique to be about 225 keV which is reasonably in good agreement with the value of 200 keV in our case (see the proposed decay scheme in Fig. 5). Purely from intensity consideration we have to assign that the 102 keV transition leads to the ground state of Eu^{153}. Consequently the capture process leading to the second excited state at ≈ 175

keV decays by the 72 keV gamma-ray; this gamma-ray can be identified with the one reported by Lee and Katz [7]) and Marty [11]) at ≈ 69 keV in the conversion electron spectrum of Sm^{153} β^--decay. If the ground to ground decay energy of Gd^{153} is ≈ 200 keV then the decay energy involving the 175 keV state must be very low, i.e., about 25 keV. From the theory of electron capture by Marshak as well as by Brysk and Rose [29]) such a low energy

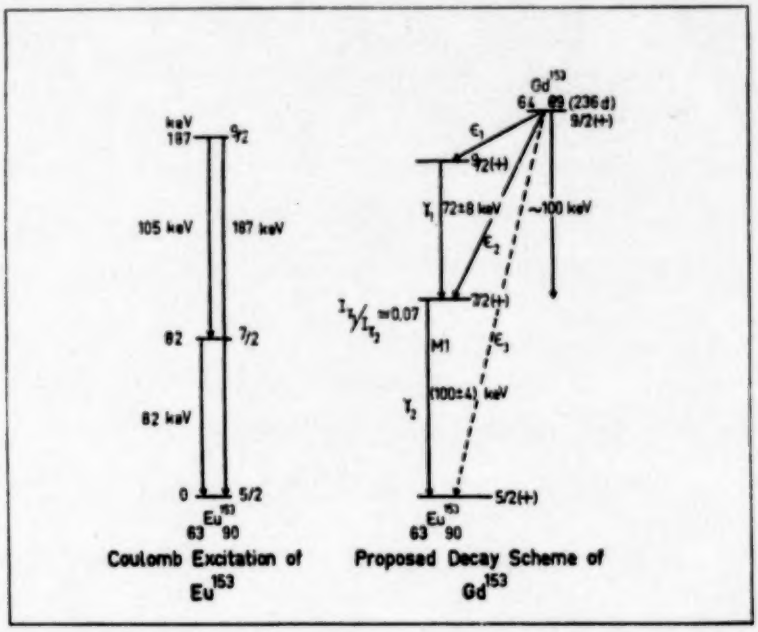

Figure 5. The proposed decay scheme of Gd^{153}. The levels in Eu^{153} reached by Coulomb excitation are shown for the sake of completeness.

capture transition must take place predominantly by L-capture (cf. K^{40} decay).

The ground state spin of Eu^{153} is measured to be 5/2 and according to shell model it should be a $d_{5/2}$ state; however, in the Schmidt diagram one finds Eu^{153} placed near the "antiparallel" region because of the experimentally determined magnetic moment value: this shows that the ground state of Eu^{153} appears to be a $f_{5/2}$ state. The maximum energy beta group from Sm^{153} has log $ft = 7.3$ which leads to Eu^{153} ground state. It is a first forbidden transition and hence requires a change of parity. Following Lee and Katz if one assigns $f_{7/2}$ to the ground state of Sm^{153} (91 neutrons) then the ground state parity of Eu^{153} is even. The first excited state at 102 keV is then 7/2 (+); it cannot presumably be 3/2 (+) since in order to make the electron capture transition to this state an allowed one we need then a lower

value of spin for the ground state of Gd^{153} also, which is probably a state of the configuration $(1h_{9/2})^7$. An assignment of 9/2 (+) as the ground state spin of Gd^{153} satisfies the above requirement; it also makes the ground-to-ground capture transitions forbidden, whereas it renders the transition to 175 keV state an allowed one ($\Delta I = 0$,No).

The 102 keV level reported here does not seem to be rotational in origin and hence cannot be easily identified with the 104 keV gamma-ray observed in Coulomb excitation[12, 13]) because of the following reasons:

(i) For pure particle transition of such low energies involved here, M1 radiation is the predominant kind; however, the strong enhancement of the E2 radiation in these collective transitions of so highly a deformed nucleus as Eu^{153} may lead to an appreciable admixture of E2 in $\Delta I = 1$ transitions and to frequent $\Delta I = 2$ cross-over transitions. Our value of α_K for 102 keV gamma-ray shows that it is mostly of M1 type, and no cross-over transition of energy $\approx$ 180 keV was observed.

(ii) Purely from intensity considerations the ordering of levels in Eu^{153} from capture decay of Gd^{153} is as shown in Fig. 5; the ordering of levels is not the same as the level order one observes in coulomb excitation of Eu^{153}.

The proposed decay scheme of Gd^{153} is based on our experimental results and is shown in Fig. 5. The levels in Eu^{153} reached by electron capture decay of Gd^{153} as is shown by our work are presumably identical with the levels that are excited by the β^--decay of Sm^{153}. The levels in Eu^{153} reached by coulomb excitation are shown for the sake of completeness.

We are gratefully indebted to Dr. R. Ramanna and Dr. S. Jha for many helpful discussions.

References

1) K. Fajans and A. F. Voigt, Phys. Rev. **60** (1941) 533
2) R. E. Hein and A. F. Voigt, Phys. Rev. **79** (1950) 783
3) J. Cork *et al*, Phys. Rev. **88** (1952) 685
4) F. K. McGowan, Phys. Rev. **93** (1954) 163
5) K. Siegbahn, M. Siegbahn Commemoration Volume p. 241
6) Bannerman, Proc. Phys. Soc. A **65** (1952) 565
7) Lee and Katz, Phys. Rev. **93** (1954) 155
8) A. W. Sunyar, Phys. Rev. **93** (1954) 163
9) Graham *et al.*, Bull. Am. Phys. Soc. **28** (1953) No. 4

10) Graham *et al.*, Bull. Am. Phys. Soc. **29** (1954) 57
11) Marty, J. de Phys. **16** (1955) 461
12) Heydenburg and Temmer, Phys. Rev. **100** (1955) 156
13) Mark and Paulissen, Phys. Rev. **100** (1955) 818
14) C. H. Pruett and R. G. Wilkinson, Phys. Rev. **96** (1954) 1340
15) Chase and Higginbotham, Rev. Sci. Instr. **23** (1953) 34
16) Johnstone, Nucleonics **11** (1953) 36
17) Reitgens *et al.*, Physica **21** (1955) 111
18) R. W. King, Rev. Mod. Phys. **26** (1954) 368
19) Mann *et al.*, Rev. Sci. Instr. **25** (1954) 1025
20) Axel, Rev. Sci. Instr. **25** (1954) 391
21) Broyles, Thomas and Haynes, Phys. Rev. **89** (1953) 715
22) K. Siegbahn, Beta and Gamma-Ray Spectroscopy (North-Holland Publishing Company, Amsterdam 1955) p. 906.
23) R. E. Marshak, Phys. Rev. **61** (1942) 431
24) M. E. Rose and I. L. Jackson, Phys. Rev. **76** (1940) 1590
25) Hill, Church and Mihelich, Rev. Sci. Instr. **23** (1952) 523
26) S. A. Moszkowski, Phys. Rev. **82** (1951) 35
27) B. L. Robinson and R. W. Fink, Rev. Mod. Phys. **27** (1955) 429
28) R. K. Gupta and S. Jha, private communication
29) H. Brysk and M. E. Rose, Oak Ridge National Laboratory Report ORNL-1830 (Jan. 13, 1955)

Nuclear Physics, North-Holland Publishing Co., Amsterdam, **1**, **(1956)**

γ-RAYS FROM THE DECAY OF Zr^{97}

R. NORDHAGEN and J. THOMASSEN
Department of Physics, University of Oslo,
Blindern, Norway

Received 12 March 1956

The fast chemical method used to separate zirconium from fission mixture and to study short-lived isotopes of zirconium [1]), made at the same time available sources of Zr^{97} with a high specific activity. To find other γ-rays than those previously known in the decay of Zr^{97}, a short search was made on these sources by the help of a 100 channel scintillation counter γ-spectrometer. A NaI (Tl) crystal of $1\frac{1}{2} \times 1\frac{1}{2}$ inch was used in the counter.

The previously known decay scheme [2,3,4]) is shown in Fig. 1A. Our results are given in Table I. The presence of the 1.02 MeV γ-ray

TABLE I

γ-rays from the decay of Zr^{97}

A: Following the 17 hour decay of Zr^{97}		
Energy in MeV	Intensity in %	Intensity in Zr → Nb decay
0.66 ± 0.01	100 ± 5	
0.75 ± 0.01	96 ± 5	96 ± 5
1.02 ± 0.03	2 ± 0.5	1 ± 0.5
1.15 ± 0.02	2 ± 0.5	2 ± 0.5
1.72 ± 0.03	0.5 ± 0.3	0.5 ± 0.3
Also two weak lines (< 0.5 %) at 1.28 and 1.77 MeV could be seen.		
B: Following the 72 minutes decay of Nb^{97}		
MeV	%	
0.66 ± 0.01	100	
1.02 ± 0.03	1 ± 0.3	

in both decay chains was proved by studying a freshly prepared source of Zr^{97}. The intensity of this line did not follow the growth of the 0.66 MeV ray from the Nb^{97} ground state activity, but was present at once. It could also be seen to grow slightly in while the

γ-rays from the Zr → Nb decay were going down in intensity. From γ-γ coincidences it was found that the 1.15 MeV ray is coincident,

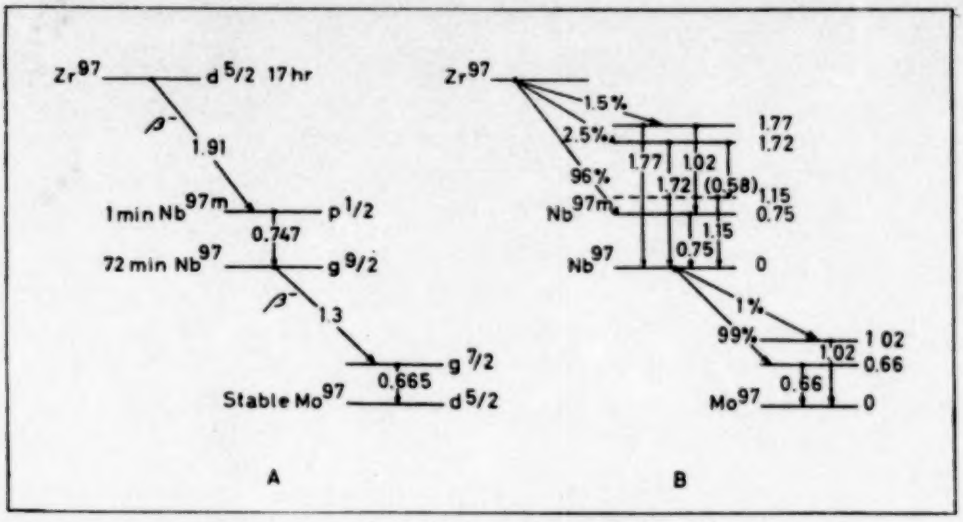

A) Decay scheme of Zr^{97} as given by previous studies [2, 3, 4])
B) Tentative decay scheme drawn from our measurements
Energies given in MeV

possibly with a ray of 0.58 ± 0.03 MeV energy. β-γ coincidences gave the same γ-spectrum as a direct measurement except for the 0.75 MeV ray. The intensity of this line was down by a factor of 5.10^{-2}. By placing $\frac{1}{2}$ mm Al in front of the β counter the lines above 1 MeV went down by a factor of 6 or more with respect to the 0.66 MeV line. The γ-rays above 1 MeV must consequently follow β-rays of lower maximum energy than those preceding the 0.66 MeV γ-ray.

We have drawn (fig. 1B) a tentative decay scheme as can be deduced from these experiments, and it is compared to the results of previous studies. The 1.28 MeV γ-ray is not shown on the figure. It is difficult to find agreement between this decay scheme and what might be expected from shell model predictions. The 1.72 MeV level might be a $g_{7/2}$ level, as expected, but as the β transitions to the levels shown will have log ft values between 7 and 8, no sure conclusions can be drawn.

References

1) A. C. Pappas and J. Thomassen (to be published)
2) W. H. Burgus, J. D. Knight and R. J. Prestwood, Phys. Rev. **79** (1950) 104
3) C. E. Mandeville, E. Shapiro, R. I. Mendenhall, E. R. Zucker and G. L. Conklin, Phys. Rev. **86** (1952) 813
4) M. Goldhaber and R. D. Hill, Rev. Modern Phys. **24** (1952) 179

Nuclear Physics, North-Holland Publishing Co., Amsterdam, **1**, **(1956)**

ON THE PENETRATING NON-IONIZING COMPONENT OF COSMIC RAYS

G. BOZÓKI, E. FENYVES and L. JÁNOSSY

Central Research Institute of Physics, Department for Cosmic Rays, Budapest

Received 13 March 1956

Abstract: Investigations into the penetrating non-ionizing component of cosmic rays were carried out with an apparatus similar to that used by Jánossy and Rochester (1943), and the results of the former experiments were substantially confirmed and extended. The collision mean free path for the non-ionizing rays, which must be assumed to consist mainly of neutrons, was found to be 270 ± 28 g/cm² in lead. This value is significantly greater than the mean value found for the primaries of penetrating showers. Problems concerning the reliability of the experimental method used are discussed.

1. Introduction

The existence of penetrating non-ionizing cosmic rays was established by Rossi and Regener [1]) at 4300 m altitude, and by Jánossy and Rochester [2]) at sea level. It was shown by Jánossy and

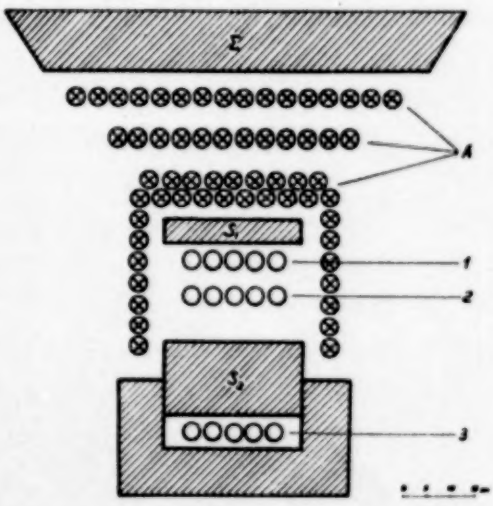

Fig. 1. The experimental arrangement. Anticoincidence counters shielding the arrangement from the front and back are not drawn. The size of the coincidence counters was 4 × 20 cm, that of the anticoincidence counters 4 × 80 cm.

Rochester that the non-ionizing radiation has a mean collision range of approximately 10 cm in lead and it was suggested that the non-ionizing rays are neutrons. Experiments on these lines were carried out also by other workers [3-7]).

In these experiments the ionizing secondaries of non-ionizing agents were detected by means of anticoincidences. The common scheme of the arrangements used in the former and present investigations is shown in Fig. 1. Anticoincidences (1,2,3,—A) are recorded. Such anticoincidences are caused mainly by the secondaries of non-ionizing primaries given rise to in the absorber S_1. Ionizing primaries are on the whole not recorded, since they cross the anticoincidence layer and thus prevent the arrangement from recording.

Our aim was to continue the measurements of Jánossy and Rochester and to measure the absorption curve of the non-ionizing particles in more detail.

2. Experimental Arrangement

The secondaries were generated in a 5 cm thick lead absorber, shown as S_1 in Fig. 1. An absorber S_2 was used to select secondaries of suitable range; in the first experiments we chose $S_2 = 15$ cm Pb (arrangement "A") and selected rather penetrating secondaries, in the later experiments $S_2 = 2.5$ cm Pb (arrangement "B") was used and thus secondaries of comparatively small penetrating power were also admitted. We measured the absorption curve of the primary non-ionizing particles by putting absorbers varying in thickness from 0 to 35 cm Pb over the anticoincidence counters.

Care had to be taken to reduce the background of spurious anticoincidences as much as possible; this was achieved by means of a large anticoincidence system consisting of 75 counters.

The background of spurious anticoincidences was measured by removing the generating absorber S_1 and by placing 35 cm Pb above the anticoincidence counters, so as to exclude any genuine anticoincidences caused by non-ionizing primaries generating secondaries in the walls of the counters or in the framework. The number of anticoincidences obtained without S_1 and $\Sigma = 35$ cm Pb give an upper limit for the background.

The following counting rates were thus obtained:

TABLE I

absorber in cm Pb	anti-coincidences	coincidences	inefficiency in %
$S_1 = 0$, $S_2 = 5+2.5$	102	155,074	0.066
$S_1 = 0$, $S_2 = 15$	287	569,954	0.050

So as to get the background count for arrangement B with $S_1 = 5$ cm Pb, $S_2 = 2.5$ cm Pb, we counted the anticoincidences with $S_1 = 0$ and $S_2 = 7.5$ cm Pb. Thus, when removing absorber S_1, we increased S_2 so as to keep the total thickness of absorber constant. In the case of arrangement A the increase of the absorber S_2 from 15 to 20 cm Pb could not be expected to affect significantly the number of background anticoincidences and therefore the background was measured simply by removing the generating absorber. The all-over efficiency of the anticoincidence system as seen from the above Table was therefore at least 99.94 %, an efficiency similar to that obtained by Jánossy and Rochester in their older measurements.

The role of the various parts of the anticoincidence shield was investigated; the details of these investigations will be published elsewhere. It was shown by these investigations that although the side shield is useful for the reduction of the background, its effect is much smaller than was supposed by Roy and Chakravarty [7]), and thus the side shield helps to measure the effects of non-ionizing rays as it reduces a comparatively small background to about half its value; it does, however, not affect the number of genuine anticoincidences in any noticeable manner. The reduction of the background is important only for the statistical evaluation of the results.

The measurements were carried out at Csillebérc, Budapest, 410 m above sea level.

3. Results

3.1. ABSORPTION OF THE NON-IONIZING RAYS MEASURED WITH ARRANGEMENT A

The results of the absorption measurements with arrangement A ($S_2 = 15$ cm Pb) are summarized in Table II, the absorption curve is plotted in Fig. 2. The full line corresponds to the absorption curve of penetrating non-ionizing rays and the dashed line to the background measured with various absorber thicknesses. The mean value of coincidences (1,2,3,) for different absorber thicknesses was 2360 c/h.

The shape of the absorption curve is similar to the absorption curve measured by Rossi and Regener [1]) who used also 15 cm Pb

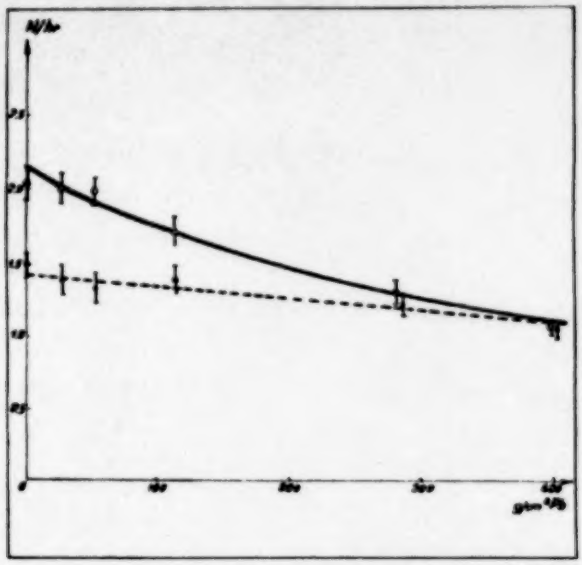

Fig. 2. Absorption curve measured with arrangement A. The full line represents the absorption curve and the dotted line the background.

between the coincidence counters. On inspecting Table II or Fig. 2 one finds that the anticoincidence rate with $S_1 = 0$ is slightly decreasing with increasing Σ; the slope of the background curve is the same within the experimental errors as the slope of the meson absorption curve. Hence we can assume that the main part of the background is due to mesons which traverse the anticoincidence trays without discharging any anticoincidence counter.

TABLE II

Absorber (cm Pb)	time (h)	(1, 2, 3, − A) total count	rate (ac/h)
$\Sigma = 0$ $S_1 = 5$, $S_2 = 15$	241	490	2.03 ± 0.09
$\Sigma = 2.5$ „ „	225	445	1.98 ± 0.09
$\Sigma = 5$ „ „	310	615	1.98 ± 0.08
$\Sigma = 10$ „ „	301	521	1.73 ± 0.08
$\Sigma = 25$ „ „	275	371	1.35 ± 0.07
$\Sigma = 35$ „ „	232	249	1.07 ± 0.07
$\Sigma = 0$ $S_1 = 0$, $S_2 = 15$	218	326	1.50 ± 0.08
$\Sigma = 2.5$ „ „	192	266	1.39 ± 0.09
$\Sigma = 5$ „ „	135	177	1.31 ± 0.10
$\Sigma = 10$ „ „	164	229	1.40 ± 0.09
$\Sigma = 25$ „ „	210	270	1.29 ± 0.08
$\Sigma = 35$ „ „	286	287	1.00 ± 0.06

As a consequence of the comparatively large background the collision mean free path of the radiation as obtained with arrangement A cannot be determined exactly. However, its value seems to be about 20 cm in Pb which is near the collision mean free path of neutrons in lead. This value of the mean free path suggests that the penetrating non-ionizing cosmic ray particles, measured with arrangement A, are mainly neutrons.

3.2. ABSORPTION OF THE NON-IONIZING RAYS MEASURED WITH ARRANGEMENT B

The absorption data obtained with arrangement B ($S_2 = 2.5$ cm Pb) are shown in Table III and Fig. 3.

The full lines in the graph are the absorption curves measured in lead and aluminium, the dashed line represents the background measured with lead absorbers. The mean value of coincidences (1, 2, 3) for different absorbers was 2490 c/h.

TABLE III

Absorber			time (h)	(1, 2, 3, −A)	
				total count	rate (ac/h)
$\Sigma =$ 0,	$S_1 = 5$ cm Pb,	$S_2 = 2.5$ cm Pb	97	786	8.10 ± 0.29
$\Sigma =$ 2.5 cm Pb	,,	,,	119	588	5.07 ± 0.21
$\Sigma =$ 5 cm Pb	,,	,,	106	425	4.01 ± 0.20
$\Sigma =$ 10 cm Pb	,,	,,	110	410	3.73 ± 0.18
$\Sigma =$ 25 cm Pb	,,	,,	202	473	2.34 ± 0.11
$\Sigma =$ 35 cm Pb	,,	,,	641	1280	2.00 ± 0.06
$\Sigma =$ 5 cm Al	$S_1 = 5$ cm Pb,	$S_2 = 2.5$ cm Pb	112	696	6.21 ± 0.24
$\Sigma =$ 10 cm Al	,,	,,	121	680	5.62 ± 0.22
$\Sigma =$ 20 cm Al	,,	,,	96.5	364	3.77 ± 0.20
$\Sigma =$ 40 cm Al	,,	,,	72	191	2.65 ± 0.19
$\Sigma =$ 0,	$S_1 = 0$,	$S_2 = 7.5$ cm Pb	70	225	3.21 ± 0.21
$\Sigma =$ 2.5 cm Pb	,,	,,	90	176	1.96 ± 0.15
$\Sigma =$ 5 cm Pb	,,	,,	84	120	1.43 ± 0.13
$\Sigma =$ 10 cm Pb	,,	,,	87	122	1.40 ± 0.13
$\Sigma =$ 25 cm Pb	,,	,,	96	135	1.41 ± 0.12
$\Sigma =$ 35 cm Pb	,,	,,	77	102	1.33 ± 0.13

The absorption curve measured in lead shows a steep decrease from $\Sigma = 0$ to $\Sigma = 5$ cm Pb and afterwards a slower exponentiallike decrease from $\Sigma = 5$ cm to $\Sigma = 35$ cm Pb. This shape of the curve is very similar to the absorption curve found by Jánossy and Rochester [2]) who used 2.2 cm Pb between the coincidence counters.

The strong decrease up to the first 5 cm of Pb is presumably caused by energetic photons generating shower particles which in their turn penetrate the relatively small lead absorber between the coincidence counters. The slower decrease after 5 cm Pb may be due to penetrating non-ionizing rays, presumably neutrons.

The background obtained with $S_1 = 0$ decreases between 0 and 5 cm Pb, but is nearly constant between 5 and 35 cm Pb. The background may be due to mesons, side showers and photons which generate shower particles in the counter walls. The counters used had 1 mm thick copper walls. Their effect is comparatively unimportant in the case of neutrons, but cannot be neglected in the case of photons. Mesons and side showers are practically not affected by the thickness of the top absorber Σ and contribute only to the nearly constant part of the background. The strong increase of background counts, if the top absorber is removed, shows the presence of photons. Direct evidence of photons producing anticoincidences in arrangement B can be furnished by measuring the absorption in light elements, e.g. aluminium. The absorption length of neutrons is expected to be approximately proportional to $A^{1/3}$, where A is the mass number of the atoms of the absorber. Hence the absorption length in lead is about twice that in aluminium, that means that neutrons are expected to be absorbed to a greater extent in aluminium layers than in lead layers of the same thickness measured in g/cm².

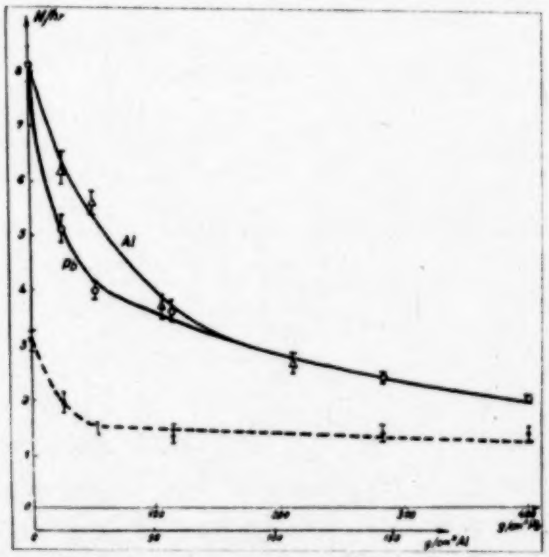

Fig. 3. Absorption curves measured with arrangement B. The full lines represent the absorption curves measured with Pb and Al, and the dotted line corresponds to the background.

The absorption of photons, however, is expected to be much stronger in lead than in aluminium. Hence, measuring the absorption in lead and aluminium, the effects of photons and neutrons can be distinguished.

From the data of Table III we find the absorption of the non-ionizing component in aluminium up to 40 cm absorber thickness. The absorption curve is plotted in Fig. 3. The lead and aluminium thicknesses denoted on the abscissa correspond to the $A^{1/3}$ relation, i.e. they are plotted in units of equivalent neutron absorption lengths.

In the case of a pure neutron radiation the two absorption curves would coincide, while, if photons as well as neutrons are present, the absorption curve measured in lead should show a steeper decrease than the curve measured in aluminium as a consequence of the rapid absorption of photons in the first few cm of lead.

As seen from Fig. 3 the measured absorption curve in lead has a much steeper first slope than the absorption curve obtained in aluminium; at great absorber thicknesses the two curves coincide as a consequence of the disappearance of photons. This effect further supports the view that the non-ionizing rays observed with arrangement B consist of photons and neutrons.

It may be seen from the lead absorption curve and the background curve measured in lead that after about 8—10 radiation lengths i.e about 5 cm of lead, the photon component practically disappears. Hence the absorption curve measured with lead absorbers of thicknesses greater than 5 cm Pb corresponds to the neutron component.

So as to determine the absorption coefficient of the neutron component it is essential to subtract from the rate of observed anticoincidences the background effect. The measurements without generating absorber S_1 show that the background rate decreases with increasing amount of absorber above the apparatus.

Combining the measurements obtained with arrangements A and B, one can fit with the method of least squares a straight line to the observed background rates. The actual calculation gives in this way a decrease of 0.86 ± 0.21 % per cm Pb for the background rate.

The coincidences (1, 2, 3) caused by mesons decrease in the same interval of absorber thicknesses by 0.684 ± 0.002 % per cm Pb. The latter value is compatible with the former, it has, however, a much smaller statistical error on account of the larger material available. As it is very probable that the background is indeed proportional to

the meson flux, we have corrected the background data using the slope obtained from the total meson flux.

Correcting the data of the lead absorption curve (Table III), the real absorption curve of neutrons in lead is obtained (Table IV).

TABLE IV

Absorber (S_1 = 5 cm Pb, S_2 = 2.5 cm Pb)	(1, 2, 3, −A) rate corrected (ac/h)
Σ = 5 cm Pb	2.49 ± 0.21
Σ = 10 „ „	2.25 ± 0.20
Σ = 25 „ „	1.01 ± 0.12
Σ = 35 „ „	0.75 ± 0.09

Plotting the curve in a semi-logarithmic scale (Fig. 4), it can be fitted by a straight line; thus the absorption curve can be expressed by

$$N(x) = N(0) \exp(-x/\bar{\lambda}_e),$$

where x is the thickness of absorber Σ in g/cm², and $\bar{\lambda}_e$ the apparent collision mean free path of neutrons. The fact that the corrected data lie inside the experimental error on an exponential curve supports the assumption that after 5 cm of lead the penetrating non-ionizing rays consist practically only of neutrons.

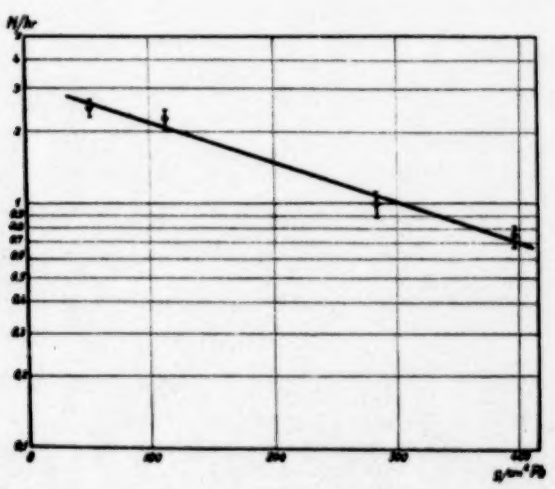

Fig. 4. Absorption of neutrons in lead measured with arrangement B. The data are corrected for the background.

Analyzing the corrected absorption curve with the method of least squares, we get

$$\bar{\lambda}_e = (270 \pm 28)\text{g/cm}^2.$$

This value is much smaller than the value given by Barton [6]), $(400 \pm 25)\text{g/cm}^2$, who used an arrangement different from ours and estimated the background in a different way. The large value of $\bar{\lambda}_e$ found by Barton might be due to the underestimation of the background.

3.3. ASSOCIATION WITH EXTENSIVE AIR SHOWERS

The association between the neutrons detected with our arrangement and extensive air showers was investigated in the following way. A counter set E of an area of 3200 cm² was placed 4 m from the centre of the neutron detector arrangement. A simple twofold coincidence apparatus measured the coincidences between the neutron detector and this counter set.

The results of this measurement are summarized in Table V. The estimated number of chance coincidences was about 3 for the total time of measurements. The total number of coincidences observed was 4, thus about the same as the expected number of chance coincidences. Taking into account statistical fluctuations three times the standard error and subtracting the background from the total number of anticoincidences (1, 2, 3, −A) measured, we can state that less than 1 % of the neutrons detected with our apparatus are accompanied by extensive showers of such density that they could be detected with the separate counter set E.

TABLE V

Absorber	Time (h)	(1, 2, 3, -A) total count	(1, 2, 3, E, -A) total count
Σ= 5 cm Pb, S_1 = 5 cm Pb, S_2 = 15 cm Pb	123.5	222	0
Σ=10 cm Pb, „ „	64.5	101	0
Σ=25 cm Pb, „ „	115	113	0
Σ=35 cm Pb, „ „	202	183	0
Σ= 5 cm Pb, S_1 = 5 cm Pb, S_2 = 2.5 cm Pb	58	217	0
Σ=10 cm Pb, „ „	84	308	0
Σ=25 cm Pb, „ „	96	202	1
Σ=35 cm Pb, „ „	107.5	224	1
Σ=20 cm Al, S_1 = 5 cm Pb, S_2 = 2.5 cm Pb	229	670	1
Σ=40 cm Al, „ „	243	733	1
Total	1322.5	2973	4

Our results concerning the correlation with extensive showers are in close agreement with the measurements of Jánossy and Rochester [2]) and Barton [2]) who, using different shower detectors, also found that the neutrons observed with their apparatus are not accompanied by showers.

Our data are not in disagreement with the well-known fact that penetrating showers are often associated with extensive air showers. Zatsepin, Sarycheva [8]), Greisen, Walker and Walker [9]) and Anishtchenko, Zatsepin, Rosenthal and Sarycheva [10]) showed namely that big penetrating showers are far more often associated with air showers than small ones and only a few percent of small penetrating showers are accompanied by those air showers which could be observed in their experiments †.

Greisen, Walker and Walker explained this in the following way. The extensive air shower detectors commonly used are sensitive for showers of densities occurring relatively near to the shower core. High-energy N-particles (nuclear interacting particles) producing big penetrating showers are more apt to be found near the core of an air shower than low-energy N-particles. Hence the probability for finding N-particles associated with air showers is greater for high-energy particles.

The neutrons detected with our apparatus have much lower mean energy than the N-particles producing penetrating showers which were observed in the experiments of Walker *et al.* Hence the expected number of neutrons associated with air showers was extremely small for our experiments in good agreement with the observed data.

4. Discussion

4.1. COMPARISON OF THE MEASURED NEUTRON INTENSITY WITH EARLIER DATA

Our absorption measurements were carried out with two arrangements: Arrangement A using 15 cm Pb between the coincidence counters similar to the measurements of Rossi and Regener, and with arrangement B using 2.5 cm Pb between the coincidence counters similar to the measurements of Jánossy and Rochester.

The intensity of penetrating non-ionizing rays measured by Rossi and Regener and by us cannot be compared in consequence of

† Similar results concerning penetrating showers and bursts produced by nuclear interactions were found later also by other authors (see ref. [11])).

the different geometrical conditions. However, the geometry of our apparatus was very similar to the geometry of the arrangement of Jánossy and Rochester. Thus we can roughly compare our data obtained with arrangement B at an altitude of 410 m with the data of the latter authors who measured practically at sea level.

Assuming a reasonable absorption length in air (120—140 g/cm²) for the neutron component, the value of the intensities measured in the two experiments agree inside the uncertainties of the comparison.

4.2. THE PHYSICAL INTERPRETATION OF THE RESULTS

In former measurements of the non-ionizing component of cosmic rays statistical accuracy of the data was so weak that no more than qualitative results could be expected. In the present investigations the statistical accuracy has been considerably improved and thus it becomes possible to analyze more critically the physical significance of the measured results.

To do this, we discuss presently the processes giving rise to anticoincidences.

Neutrons and charged N-rays are falling on the top absorber Σ. Three kinds of neutrons emerge from the absorber Σ: a) neutrons traversing the absorber without inelastic collision, b) neutrons

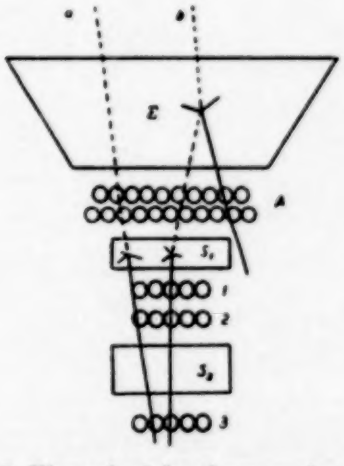

Fig. 5. The principle of measuring the collision mean free path.

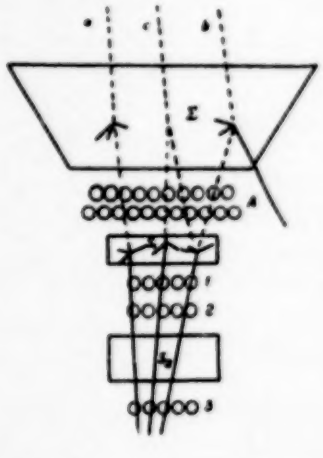

Fig. 6. Systematic errors in measuring the collision mean free path.

suffering inelastic collision in the absorber Σ and c) neutrons generated in the absorber Σ by charged or neutral N-particles. The two latter groups can be regarded as neutrons generated in nuclear interactions in the absorber Σ.

An idealized picture of the processes giving rise to the anticoin-

cidences measured is the following. The probability for a neutron to traverse the absorber Σ of thickness x without inelastic collision is $\exp(x/\lambda_e)$, where λ_e is the collision mean free path; in the latter case the neutron behaves as if the absorber Σ were not there (Fig. 5, particle *a*).

On the other hand neutrons generated in the absorber Σ are prevented from giving rise to anticoincidences because the ionizing particles usually produced simultaneously with the neutron discharge the anticoincidence tray (Fig. 5, particle *b*). Assuming that *each* neutron generated in the absorber is associated with such ionizing particles, we expect the rate of anticoincidences to decrease exponentially with the thickness x of absorber Σ, thus

$$N(x) = N(0) \exp(-x/\lambda_e).$$

The actual process is, however, more complicated and the interpretation of the experimentally determined absorption curve needs some comment.

Neutrons generated in the absorber Σ can give rise to anticoincidences if the ionizing particles produced simultaneously are absorbed in Σ (Fig. 6, particle *a*), or if they miss the anticoincidence counters (Fig. 6, particle *b*), or if ionizing particles are not produced at all (Fig. 6, particle *c*).

Such events may give rise to anticoincidences and therefore we have for the coefficient in the exponent of the measured absorption curve, which we shall call the apparent collision mean free path,

$$\bar{\lambda}_e > \lambda_e,$$

as it does not include all types of possible inelastic collisions.

If we neglect for the moment the process in which ionizing particles miss the anticoincidence tray, the observed collision mean free path corresponds to collisions in which ionizing secondaries capable of penetrating the remaining absorber thickness are produced.

Estimating the minimum energy loss $E_{\min}$ required to give rise to such penetrating secondaries, we can say roughly that $\bar{\lambda}_e$ is the collision mean free path corresponding to losses $E > E_{\min}$. $E_{\min}$ is of course not sharply defined, partly because of the fluctuation of the distribution of the energy among the secondaries and also because different energies are required to give rise to secondaries penetrating the rest of Σ depending on the layer of Σ in which the collision takes place.

The difference between λ_c and $\bar{\lambda}_c$ is expected to be particularly large for low-energy primaries, as such primaries have a small chance only to give rise to secondaries penetrating 10 cm Pb or more; for higher energies the difference may decrease.

More accurate calculations of these effects could be carried out, the accuracy of the present measurements, however, does not justify such calculations.

The absorber thickness which must be traversed by the ionizing secondaries varies roughly from 5 cm to 35 cm Pb or more. The corresponding minimum energy of a proton is $2-8\times 10^8$eV and for a π-meson $1-5\times 10^8$eV. Taking into account the rest energy of the π-meson, the minimum energy loss in such collisions is

$$E_{\min} \approx 2-8 \times 10^8\text{eV}.$$

Considering that this energy is usually distributed among several particles including neutral particle, we see that the above picture is only a very rough approximation.

The results could be exactly interpreted by investigating how variation of the absorbers S_1 and S_2 affects the anticoincidences. Even more straightforward results could be obtained by slicing the absorber Σ into a number of layers and placing counters into the gaps as has been done by Azimov, Dobrotin, Ljubimov and Ryshkova [12]). Investigations of this kind are in preparation.

The mean free path, to be understood in the sense discussed above obtained from our data, is thus

$$\bar{\lambda}_c = (270\pm 28)\text{g/cm}^2.$$

This value is significantly greater than the collision mean free path in lead of penetrating shower-producing N-rays as measured by several authors [13–16]) (see Table VI). The mean value found from their data,

$$\lambda_c = (158\pm 6)\text{g/cm}^2,$$

is very close to the geometrical mean free path (164 g/cm^2).

The estimated mean energy of N-particles observed in the experiments shown in Table VI is about 15—50 GeV [17]). It seems very probable that in this high-energy region the method for measuring the collision mean free path discussed above may give values nearer to λ_c than we obtained in our measurements with lower energy neutrons.

TABLE VI

Experiment	λ_e (g/cm^2)
Walker [13]) charged N-rays (average)	158±8
Walker *et al.* [14]) charged N-rays neutral N-rays	 157±12 164±15
Sitte [15]) charged N-rays (average)	175±8
Boehmer and Bridge [16]) neutral N-rays	143±30[a])
Mean value	158±6 [b])

a) Value measured with highest multiplicity of secondaries.
b) The standard error might be somewhat greater due to systematic errors in the individual measurements[17]).

The mean energy of the neutrons observed in our measurements may be estimated to be of the order of 1 GeV only, the estimate being based on the threshold energy of the apparatus and on the expected neutron intensity [17]).

Although the difference between our large value of $\bar{\lambda}_e$ and the smaller values obtained in experiments using higher energies might be at least partly accounted for by the effects discussed above, the difference is so large that one might also suspect that the collision cross section has a real increase with energy.

Measurements carried out with synchro-cyclotrons and cosmotrons showed an increase of the total cross section of nucleon-nucleon collisions with increasing energy above 0.4 GeV [18, 19]). Corresponding to these results the cross sections (σ_i) for inelastic collisions of neutrons with nuclei seem to increase also with energy[20]).

TABLE VII

	λ_e(g/cm^2)	σ_i(barn)
High energy cosmic ray measurements ($E \approx$ 15—50 GeV, charged and neutral N-rays)	158±6	2.18±0.08
Cosmotron measurements[18]) (1.4 GeV neutrons)	199±5	1.73±0.04
Present experiments	270±28	1.27±0.13

The increase of the inelastic cross section or the decrease of the collision mean free path with the energy of the particles may be shown more definitely by comparing the results of accelerator and cosmic ray experiments [17]) (Table VII). The collision mean free path in lead of the 1.4 GeV neutrons generated in the Brookhaven cosmotron [19]) is much greater than the collision mean free path of cosmic ray neutrons having mean energies between 15 and 50 GeV.

However, it is shown in Table VII that the collision mean free path measured in our experiments is also greater than the cosmotron value, the difference being about 2,5 times the standard error, although the mean energy of neutrons detected with our apparatus might be near to the energy of the neutrons used in the cosmotron. Hence it seems likely that the great value of $\bar{\lambda}_e$ observed in the present experiments is only partly due to the energy dependence of the collision mean free path.

Further investigations to clear this question are in progress.

References

1) B. Rossi and V. Regener, Phys. Rev. **58** (1940) 837
2) L. Jánossy and G. Rochester, Proc. Roy. Soc. A **181** (1943) 399
3) S. C. Sirkar and S. Ghosh, Proc. Nat. Inst. Sci. **8** (1942) 233
4) S. C. Sirkar and P. K. Bhattacharyya, Science and Culture **8** (1942) 89
5) S. C. Sirkar and P. K. Bhattacharyya, Proc. Nat. Inst. Sci. **10** (1944) 175
6) J. C. Barton, Proc. Phys. Soc. A **64** (1951) 1042
7) S. B. Roy and R. Chakravarti, Ind. Journ. Phys. **37**(1954) 167
8) G. T. Zatsepin and L. I. Sarycheva, DAN **69** (1949) 639
9) K. Greisen, W. D. Walker and S. P. Walker, Phys. Rev. **80** (1950) 535
10) J. Anishtchenko, G. T. Zatsepin, I. L. Rosenthal and L. I. Sarycheva, JETP **22** (1952) 143
11) K. Greisen and W. D. Walker, Phys. Rev. **89** (1953) 915
12) S. A. Azimov, N. A. Dobrotin, A. L. Ljubimov and K. P. Ryshkova, Izv. A. N. SSSR **17** (1953) 80
13) W. D. Walker, Phys. Rev. **77** (1950) 686
14) W. D. Walker, S. P. Walker and K. Greisen, Phys. Rev. **80** (1950) 545
15) K. Sitte, Phys. Rev. **78** (1950) 714
16) H. W. Boehmer and H. S. Bridge, Phys. Rev. **85** (1952) 863
17) R. W. Williams, Phys. Rev. **98** (1955) 1393
18) A. M. Shapiro, C. P. Leavitt and F. F. Chen, Phys. Rev. **95** (1954) 663
19) T. Coor, D. A. Hill, W. F. Hornyak, L. W. Smith and G. Snow, Phys. Rev. **98** (1955) 1369
20) F. F. Chen, C. P. Leavitt and A. M. Shapiro, Phys. Rev. **99** (1955) 857

Nuclear Physics, North-Holland Publishing Co., Amsterdam, **1 (1956)**

ON THE ANOMALOUS L-X-RAY YIELD IN LIGHT MESIC ATOMS

M. DEMEUR

CERN, *Theoretical Study Division*
at the Institute for Theoretical Physics,
University of Copenhagen

Received 24 February 1956

Abstract: The properties of a cascade with $\Delta n = 1$ and $\Delta l = \pm 1$ are investigated. It is shown that, if the initial distribution is a statistical one (i.e. proportional to $(2l+1)$), accumulation occurs in the states of intermediate angular momentum. Application is made to the case of π-Carbon, starting with a statistical distribution on the states $n = 17$.

1. Introduction

Since the observation of slow electrons at the end of meson tracks in nuclear plates [1]) attention has been paid to the role of Auger effect in the structure of mesic atoms [2,3]). More recently another problem arose in the same field with the discovery of an anomalously low yield of photons of the L-series in light π-mesic atoms.

The decrease of the L-yield with decreasing Z must find an explanation rather in the atomic structure of the system than in a nuclear interaction. Overlapping of the wave-functions of the nucleons and of the meson occurs indeed less and less with decreasing Z. Besides, the authors quoted in ref. [4,5]) mention an anomalous L-yield in μ-mesic atoms also, showing that the phenomenon is not related to a strong nuclear interaction.

As in previous works [2,3]), the mesic atom will be considered here as a hydrogenic one. It will be supposed that the meson is captured in an initial orbit (n_i, l) with a probability distribution $D_{n_i l} = (2l+1)/n_i^2$, the value of n_i being given by $\varkappa^{1/2}\nu$ where $\varkappa$ is the meson mass measured in electron mass unit, and ν is the principal quantum number of the electronic shell in the region of which the meson is captured. From its initial state (n_i, l) the meson jumps by radiative or Auger transitions to states of lower n until it reaches a state of large overlap with the nucleus giving rise to a star (in the case of the

π-meson and of the μ-meson in heavy elements). In the case of capture by a light element the μ-meson decays after having reached the 1s state (or the 2s state if it is metastable). Moreover it will be admitted that a vacancy in an electronic shell is quickly replenished, and that a highly ionised atom captures external electrons in a short time.

Part of the cascade consists in a succession of Auger transitions with $\Delta n = n_1 - n_2 = 1$. The properties of a cascade of that type are examined in § 3, and an application to the L-yield of the π-C atom is presented in § 4.

2. Radiative and Auger Transitions

The evaluation of these transition probabilities has been presented by Burbidge and de Borde[2,3]). Nevertheless it will be sketched again in order to define the approximation adopted. The matrix element attached to the transition of a meson of initial and final bound states (n_1, l_1, m_1) and (n_2, l_2, m_2), ejecting an electron of initial bound state $(\nu_1, \lambda_1, \mu_1)$ to a free state (p, λ_2, μ_2) is given by

$$M = \int \mathrm{d}^3u\, \psi^{\mu_2 *}_{\lambda_2}(p,u)\, \psi^{\mu_1}_{\nu_1\lambda_1}(u) \int \mathrm{d}^3v\, \psi^{m_2 *}_{n_2 l_2}(v)\, \psi^{m_1}_{n_1 l_1}(v)\, r^{-1}$$

where a) u and v are the coordinates of the electron and of the meson, respectively,

b) the functions $\psi^{\mu}_{\lambda}(p,u)$ and $\psi^{m}_{nl}(v)$ are a coulomb wave-function of positive energy (momentum $p\hbar$ and orbital momentum λ) and a hydrogenic wave-function with quantum numbers nlm, respectively,

c) $r^{-1} = \Sigma_{N=0}^{\infty} \Sigma_{M=-N}^{N} [(N-|M|)!/(N+|M|)!] Y_N^{M*}(\omega_u)\, Y_N^M(\omega_v)\{\}$ where $\{\} = v^N/u^{N+1}$ if $v < u$ and u^N/v^{N+1} if $v > u$; ω_u and ω_v represent the angular variables of electron and meson.

The transition probability between mesic states (n_1, l_1, m_1), and (n_2, l_2, m_2) can be expressed in angular and radial parts:

$$P(\nu_1, \lambda_1; \lambda_2) = (e^2/\hbar)^2 |M|^2 = (e^2/\hbar)^2 \Omega(\lambda_1, \lambda_2) |I(\nu_1, \lambda_1; \lambda_2)|^2,$$

the angular part Ω containing a summation over all magnetic quantum numbers, and the radial part I being given by

$$I(\nu_1, \lambda_1; \lambda_2) = \int \mathrm{d}u\, u^2 R_{\lambda_2}(p,u) R_{\nu_1\lambda_1}(u) \left[u^{-(N+1)} I_N + J_N(u)\right]$$

† The quantity $\varkappa^{1/2}$ is equal to 15, 17, 31, and 51 if the meson is a μ, π, τ, or Ξ meson.

with

$$I_N = \int_0^\infty \mathrm{d}v\, v^{2+N} R_{n_2 l_2} R_{n_1 l_1}$$

and

$$J_N = \int_u^\infty \mathrm{d}v (u^N/v^{N-1} - v^{N+2}/u^{N+1}) R_{n_2 l_2} R_{n_1 l_1}$$

where the R's are the radial parts of the ψ's.

The approximation that neglects $J_n(u)$ against $u^{-(N+1)} I_n$ makes the Auger transition probabilities proportional to the corresponding radiative ones: the I_n's are the radial parts of the radiative matrix elements.† In fact, the transitions are mainly of the electric dipole type ($N=1$).

The validity of this approximation can be shown qualitatively if attention is paid to the terms J_n that measure the overlap of meson and electron wave functions. In both cases of Auger effect in the K- and L-shells the upper limit of the average value of the radial coordinate of the meson $\bar{v}$ is one fourth of the average value of the radial coordinate of the electron $\bar{u}$. This consequence of the large meson mass ensures that the correction to the adopted approximation remains small, and shows that the mesic Auger effect is a phenomenon closer to internal conversion than to the atomic Auger effect ††.

In the case $N=1$ the Ω's for complete subshells, summation over all magnetic quantum numbers being performed, are given in Table I, where $\omega_\pm$ refer to transitions between l_1 and $l_2 = (l_1 \pm 1)$

TABLE I

Angular part $\Omega(\lambda_1;\lambda_2)$ of the Auger transition probability (E1)

Ejected electrons	$\lambda_2 = 0$	1	2
Bound electrons			
$(ns)^2$: $\lambda_1 = 0$	—	$\omega_\pm$	—
$(np)^6$: $\lambda_1 = 1$	$\omega_\pm$	—	$2\omega_\pm$

states, and are given by

$$\omega_+ = \frac{2(l_1+1)}{3(2l_1+1)} \quad \text{and} \quad \omega_- = \frac{2l_1}{3(2l_1+1)}.$$

† This approximation cancels the monopole transitions (called S transitions in ref. [2]), for I_0 vanishes by orthogonality.

†† The correction due to J_1 has been evaluated by de Borde [3]) in case of the K-shell and is indeed small.

The Ω's of the corresponding radiative transitions being equal to $\omega_{\pm}/2$, the ratio of the Auger to the radiative transition probabilities will be simpler than each of them separately.

In case of Auger transitions in the K- and L-shells we get the following ratios of probabilities:

$$\frac{P_K}{P_R} = 64\pi \left(\frac{\hbar c}{e^2}\right)^3 \frac{Z_1^2}{Z^6} \frac{x^2}{1+x^2} \frac{\exp[x(4\,\mathrm{arctg}\, x - \pi)]}{\sinh \pi x} (\varkappa N_{12})^{-3}, \tag{1}$$

$$\frac{P_L}{P_R} = 32\pi \left(\frac{\hbar c}{e^2}\right)^3 \frac{Z_1^2}{Z^6} \frac{x^2(4+3x^2)(4+5x^2)\exp[x(4\,\mathrm{arctg}\, \frac{x}{2} - \pi)]}{\sinh \pi x} (\varkappa N_{12})^{-3}, \tag{2}$$

where $P_K = P(1,0;1)$, $P_L = P(2,0;1) + P(2,1;0) + P(2,1;2)$ and P_R is the radiative transition probability; x is related to the electron momentum p by $x = Z_1\hbar/a_0 p$, Z_1 being the effective charge acting on the electron. We have

$$p^2 = 2m[(\varkappa N_{12} Z^2 e^2/2a_0) - \varepsilon] \tag{3}$$

where Z is the charge acting on the meson; N_{12} characterizes the meson transition: $N_{12} = 1/n_2^2 - 1/n_1^2$; $\varepsilon = \varepsilon_\nu = Z_1^2 e^2/2a_0\nu^2$ is the electron binding energy in the ν-shell.

The ratios P_K/P_R and P_L/P_R are analogous to the non-relativistic conversion coefficients $\alpha_K(E1)$ and $\alpha_L(E1)$. $Z = Z_1$ makes them identical with these coefficients. The formula (2) has been compared with those of Hebb and Nelson [7]). The general properties of the internal conversion are applicable here: thus the 2s electrons are responsible for the major part of the L conversion; conversion in the M-shell will be relatively unimportant except if the energy is below ε_2.

When ε is negligible, we have $x = (\varkappa N_{12})^{-\frac{1}{2}} Z_1/Z$. Thus, in case of very energetic transitions x becomes $\ll 1$, and we have

$$P_K/P_R = 64(\hbar c/e^2)^3 (Z_1^3/Z^7) (\varkappa N_{12})^{-7/2}, \tag{4}$$

$$P_K/P_L = 8, \tag{5}$$

which gives the total Auger probability

$$P_A = 72 \left(\frac{\hbar c}{e^2}\right)^3 (Z_1^3/Z^7) (\varkappa N_{12})^{-7/2} P_R. \tag{6}$$

The relation (5) was known since the early development of the theory of internal conversion [8]), and represents simply the ratio of K and L electron presence in the centre of the atom. The elimination

of $\varkappa N_{12}$ between the energy of the Auger electron and relation (6) gives

$$P_A/P_R \approx 55 Z_1^3 E_{keV}^{-7/2}$$

where E_{keV} is the energy measured in keV. This last expression shows that the emission of electrons of great energy is unlikely whatever the meson mass is. In fact, such electrons have never been observed.

The regions of the cascade where the Auger transitions are energetically possible in a given shell, and for a given $\Delta n = n_1 - n_2$, are determined by the condition $p^2 > 0$ or according to formula (3) by†

$$\varkappa N_{12} Z^2 > (Z_1/\nu)^2.$$

In the case $\Delta n = 1$, we get the upper limit for n_1 given by Table II,

TABLE II

	$Z = 6$	12	35
$\nu = 1$	10	9	9
2	23	16	14
3	—	43	23
4	—	—	35

the electronic binding energies being evaluated by means of the charge $Z_1 = Z^* - 1$, where Z^* is Slater's effective charge, and -1 takes account of the screening due to the meson.

In fact, the probabilities P_A (and P_R) being related to the transition $(n_1, l_1) \to (n_2, l_2)$, might be written $P_{A,R}\ (n_1, l_1; n_2, l_2)$. If we define a function

$$f(n_1, l_1) = \sum_{n_2 l_2} P_A(n_1, l_1; n_2, l_2) / \sum_{n_2 l_2} P_R(n_1, l_1; n_2, l_2),$$

the lower limit of the regions where the Auger transitions are more frequent than the radiative ones, is given by the condition $f = 1$. An estimate of these limits can be deduced from figure 1 of de Borde's paper [3]) if use is made of the fact that f is proportional to Z^{-4} (cf. (6)). We then get $f \approx 1$ for the n_1 values given in Table III.

Among the Auger transitions those with $\Delta n = 1$ are the most probable since P_A is proportional to the square of the integral I_1 which decreases when Δn increases, the functions $R_{n_1 l_1}$, and the

† The condition must be written separately for every subshell higher than 3p. In the case of light atoms that distinction is not necessary.

$R_{n_1 l_1}$ offering less and less overlap. Moreover, P_A is proportional to the inverse of the square root of the energy (if that energy is not too close to the threshold).

TABLE III

	$l_1 = 1$	$l_1 = n_1 - 1$
$Z = 6$	$n_1 = 4$	3
12	7	4
35	12	6

The quantum numbers n_1 and l_1 characterize mesic states with equal possibilities of decay by radiative and Auger transitions.

On the other hand the radiative possibilities increase with Δn, since the I_1^2 dependence is more than compensated by the increase of the transition probability with the cube of the energy.

From this the conclusion may be drawn that the following qualitative description of the behaviour of the meson after capture in a bound state can be given: at first the meson performs a cascade of Auger transitions; then, when the function f approaches unity, the radiative transitions take over with large Δn. The properties of the cascade vary rapidly as a function of Z. For instance the region of the cascade where the dominant transition is of the Auger type with $\Delta n = 1$ is two or three times larger in the case of Carbon (from $n \approx 23$ to $n \approx 6$) than in Magnesium (from $n \approx 16$ to $n \approx 9$).

3. Cascade with $\Delta n = 1$

The cascade with $\Delta n = 1$ can be investigated without evaluation of the transition probabilities themselves. In every state (n,l) we want to know the ratio

$$S_{nl} = \frac{P(n,l;n-1,l-1)}{P(n,l;n-1,l+1)}.$$

In the approximation adopted here S_{nl} is the same in the case of both Auger and radiative transitions and is given by

$$S_{nl} = \frac{\omega_-}{\omega_+}\left(\frac{I_1(n,l;n-1,l-1)}{I_1(n,l;n-1,l+1)}\right)^2 = \frac{l}{l+1}\left(\frac{I_1(n,l;n-1,l-1)}{I_1(n,l;n-1,l+1)}\right)^2.$$

The integral I_1 is a well-known expression calculated by Gordon [9]). Applying the recurrence relations [10]) between hypergeometric

functions, one obtains S_{nl} expressed by two ${}_2F_1$ functions only:

$$S_{nl}=\frac{l(n+l)(n-l-2)}{(l+1)(n+l-1)(n-l-1)}\left[\frac{\frac{n-l}{2n-1}\,{}_2F_1(a,b,c,z)+a\,{}_2F_1(a+1,b,c,z)}{\frac{n+l+1}{2n-1}\,{}_2F_1(a,b,c,z)+a\,{}_2F_1(a+1,b,c,z)}\right]^2 \tag{7}$$

where $a=l+1-n$; $b=l+2-n$; $c=2l+2$; $z=-4n(n-1)$. It is easily verified that $S_{n0}=0$, $S_{n,n-1}=S_{n,n-2}=\infty$. The first significant S_{nl} is then S_{41}.

If we express $S_{n,l-1}$ as a function of the ${}_2F_1$ appearing in (7), it is possible to eliminate the ratio

$${}_2F_1(a+1,b,c,z)/{}_2F_1(a,b,c,z)$$

between $S_{nl}^{1/2}$ and $S_{n,l-1}^{1/2}$ and to obtain the recurrence formula

$$S_{n,l-1}^{1/2}=-\alpha_{nl}\frac{\beta_{nl}S_{nl}^{1/2}+\gamma_{nl}}{\delta_{nl}S_{nl}^{1/2}+\varepsilon_{nl}} \tag{8}$$

where $\alpha_{nl}=(l-1)^{1/2}(n+l-2)^{-1/2}(n-l)^{-1/2}$

$\beta_{nl}=l^{1/2}(l+1)^{1/2}[4(n^2-l^2)(n-1)^2-2n+1]/2n^2$

$\gamma_{nl}=(n+l)^{1/2}(n+l-1)^{1/2}(n-l-1)^{1/2}(n-l-2)^{1/2}$

$\delta_{nl}=(l+1)^{1/2}(n+l-1)^{1/2}(n-l-1)^{1/2}$

$\varepsilon_{nl}=2l^{3/2}(n+l)^{1/2}(n-l-2)^{1/2}$.

When replacing l by $(n-3)$ in (8) we obtain an explicit expression for $S_{n,n-3}$, $S_{n,n-2}$ being infinite,

$$S_{n,n-3}=(n-3)(2n-3)(8n^2-12n+5)^2/16n^4.$$

This formula is the starting point† of the application of eq. (8) in order to obtain the remaining S_{nl}.

For very large values of n and $n\gg l$ the S_{nl} tend to the limit

$$\omega_-/\omega_+=l/l+1.$$

In that case a probability distribution $D_{nl}=(2l+1)/n^2$ (statistical distribution) is conserved:

$$\begin{aligned}D_{n-1,l}&=D_{n,l-1}(1+S_{n,l-1})^{-1}+D_{n,l+1}S_{n,l+1}(1+S_{n,l+1})^{-1}\\&=(2l+1)/n^2=D_{nl},\end{aligned}$$

† In order to start with S_{n0} rather than with $S_{n,n-2}$, one should remove the indetermination of $S_{n0}^{1/2}/\alpha_{n1}$ which leads to evaluation of the ${}_2F_1$'s appearing in S_{n0}. The extension of the present scheme to the case of $\Delta n>1$ is obvious.

n \ $l=$	1	2	3	4	5	6	7	8	9	10	11	12	13	14
17	.829	1.55	2.45	3.71	5.55	8.31	12.5	19.3	30.8	51.1	90.1	177	416	1451
16	.856	1.64	2.65	4.13	6.35	9.8	15.4	25	42	75.1	149	352	1246	
15	.89	1.74	2.91	4.65	7.38	11.8	19.4	33.7	61.2	123	294	1056		
14	.925	1.87	3.23	5.39	8.92	15.1	26.4	48.9	100	243	882			
13	.975	2.04	3.67	6.36	11.1	19.9	37.8	78.7	197	725				
12	1.03	2.25	4.28	7.86	14.6	28.5	61.1	155	584					
11	1.11	2.56	5.12	10.1	20.5	45.3	118	459						
10	1.22	3	6.46	13.9	32.3	87.1	349							
9	1.36	3.66	8.72	21.5	61.1	255								
8	1.58	4.78	13.2	39.7	176									
7	1.92	6.73	23.3	112.2										
6	2.54	11.53	63.6											
5	3.91	29.4												
4	8.81													

TABLE IV

The ratios $S_{nl} = P(n,l;n-1,l-1)/P(n,l;n-1,l+1)$ are given until $n = 17$. The S_{nl} are less than unity for $n > 12$; their asymptotic value is 1/2.

but is smaller than the statistical distribution of the $(n-1)$ shell, which has the value† $(2l+1)/(n-1)^2$.

For very large values of n and $n_r = n-l-1 \ll n$ the S_{nl} tend to the limit

$$S_{n,n-1-n_r} = 16n^2/n_r(n_r-1)$$

which is always very large. In that case one has the relation $D_{n-1,l-1} \approx D_{nl}$ expressing that any distribution is conserved.

It results that, for large values of n, a cascade with $\Delta n = 1$ which starts with a statistical probability distribution, conserves that distribution in the case of small and large values of the angular momentum, and leads, in consequence, to an accumulation in the states of intermediate values of l.

When n is not very large compared with unity, and when l is small, the S_{nl} differ considerably from the classical limit $l/l+1$ as can be seen from Table IV. When n_r is small, S_{nl} always remains large. It is shown in § 4 that, even in the case of small n's, the final probability distribution presents an accumulation in the states of intermediate values of l.

For the application to atomic spectroscopy some integrals I_1 have been computed by evaluation of the ${}_2F_1$ functions [11,12]). The values of some S_{nl} can be deduced from these and are compared in Table V with the values obtained from the recurrence formula.

TABLE V

Comparison of values of some ratios S_{nl}

S_{nl}	Kupper[12])	Slack[11])	Table IV
41	8.81	8.81	8.81
52	28.4	29.5	29.4
51	3.96	3.91	3.91
63	63.4	65.6	63.6
62	10.15	14.6	11.5
61	4.38	2.3	2.54
74	112.2	95.5	112.2
73	23.4	26.5	23.3
72		8.2	6.73
71		1.62	1.92

† That statement is only valid if the correction of order l/n to $l/l+1$ vanishes. It is shown in the Appendix that this is indeed the case.

4. Application to the Mesic Atom π-Carbon

The cascade performed by a π meson captured in a Carbon atom has been computed as follows: assuming a statistical distribution in $n = 17$ (the region of the electronic K-shell) a cascade of $\Delta n = 1$ transitions is adopted until $n = 6$ (cf. § 2); then, by means of radiative transition probabilities P_R established for atomic spectroscopy, and using the P_A/P_R ratios given in § 2, the cascade is studied until $n = 2$.

After the first step ($\Delta n = 1$ cascade ending in $n = 6$) we obtain the following distribution D_{6l} (called DI):

$$\left.\begin{array}{ll} D_{60} = 13.5\,\% & D_{63} = 14.8 \\ D_{61} = 26.4 & D_{64} = 12.3 \\ D_{62} = 21.2 & D_{65} = 11.7 \end{array}\right\} DI$$

which shows accumulation in p and d states, and differs considerably from the distributions proposed by Platt *et al.* [6]: †

$$\begin{array}{ll} D_{6l} = 1/6 & D\text{II} \\ D_{6l} = (2l+1)/36 & D\text{III} \\ D_{6l} = l^2/55 & D\text{IV}. \end{array}$$

The accumulation in p and d states is best shown if one starts in $n = 17$ with a constant distribution, for in that case one gets

$$\begin{array}{ll} D_{60} = 18.8\,\% & D_{63} = 10.7 \\ D_{61} = 36.1 & D_{64} = 7 \\ D_{62} = 21.2 & D_{65} = 6.1. \end{array}$$

If we call α_l the emission probability of a photon of the L-series by a meson starting from a($6l$) state, the L-X-ray yield r_L will be given by $r_L = \Sigma_0^5 D_{6l}\alpha_l$. Similarly, if we call β_l the emission probability of the L_α-line, the L_α-X-ray yield $r_{L\alpha}$ will be given by $r_{L\alpha} = \Sigma_0^5 D_{6l}\beta_l$. This second step of the cascade has been computed with the assumption that the meson is absorbed by the nucleus when it reaches the 5s, 4s, and 3s states.

Table VI presents the α_l's in the case of Carbon and Magnesium and the β_l's in the case of Carbon.

† I am indebted to Professor J. B. Platt for sending me a preprint of his paper [6]).

TABLE VI

$Z = 6$				$Z = 12$	
α_0	11%	β_0	4	α_0	21
α_1	6	β_1	3	α_1	14
α_2	15	β_2	5	α_2	25
α_3	17	β_3	10	α_3	59
α_4	45	β_4	17	α_4	81
α_5	86	β_5	86	α_5	100

The α_l's are the emission probabilities of a photon of the L-series by a meson starting from a $(6l)$ state. The β_l's are the probabilities of emission of the L_α-line under the same conditions.

We then get the following yields:

TABLE VII

Distribution	$Z = 6$		$Z = 12$
	r_L	$r_{L\alpha}/r_L$	r_L
DI	24%	66	42
DII	30	69	51
DIII	44	77	67
DIV	56	82	80
Experimental [6])	18±6	79±28	(66)

r_L represents the probability of emission of one photon of the L-series in the case of a statistical distribution of mesons over the states of principal quantum number $n = 17$.
$r_{L\alpha}$ is the same quantity but related to the emission of the L_α-line.

In the case of Carbon the yield r_L obtained by the use of distribution DI is the best. The experimental error in $r_{L\alpha}$ is so large that no useful conclusion may be drawn at the present time. It is difficult to estimate how far the statistical distribution assumed in $n = 17$ is modified by the capture of mesons in the region of the electronic L-shell, and how far in consequence the above calculated yields are changed.

As was expected, the distribution DI does not fit the case of Magnesium since for $Z = 12$ the Auger cascade is of less importance (cf. above § 2). The deviation from the statistical distribution should thus be smaller, and indeed the distribution DIII seems to be the best in this case. Similar conclusions may be drawn from the results of Platt *et al.* [6]) for Oxygen and Aluminium.

The observation of mesic Auger electrons has led de Borde to the

conclusion that in Bromine the probability distribution in $n = 17$ seems to peak towards the low values of the angular momentum. This may be the consequence of meson capture in the L-shell, followed by a cascade with $\Delta n = 1$ down to $n = 17$.

It must be pointed out that any failure in the validity of the assumptions about replenishment of vacancies and capture of external electrons will lead to an increase in the radiative yields. In some way, the fact that the above result is close to the experimental value of the L-yield is an indication that both assumptions are fulfilled to a good approximation.

5. Photo-electric absorption of mesic X-rays in target

Another phenomenon connected with the high mass of the meson, is the photo-electric absorption of the mesic X-rays in the target itself. Such an effect is, of course, impossible in the case of ordinary X-rays, the photon energies being smaller than the electron binding energies.

The photo-electric absorption coefficient is given by the well-known formula [13])

$$\tau_K = N\phi_0 2^{5/2} Z^5 (e^2/\hbar c)^4 (mc^2/k)^{7/2} \tag{9}$$

adapted to our case since ε_1 is negligible, and relativity effects may be neglected (in the case of light elements). In formula (9) we have used the notation

$$\phi_0 = (8\pi/3) \cdot (e^2/mc^2)^2$$

and N denotes the number of atoms per cm^3.

If we replace k by its value $\varkappa N_{12} Z^2 e^2/2a_0$ we get

$$\tau_K = N\phi_0 64 (\hbar c/c^2)^3 Z^{-2} (\varkappa N_{12})^{-7/2},$$

while if the absorption takes place in another element Z_2, the coefficient varies as

$$\tau_K(Z_2) \propto Z_2^5 Z^{-7}.$$

With correction for photo-electric absorption in the L-shell, the value of τ in the case of the 3d—2p line in π-mesic Carbon is† 1.16 cm^{-1} which indicates that the absorption will be large in a 1″ thick target.

In heavier elements, such as Iron, the Compton effect in the target becomes overwhelming.

† Graphite of density 2.25; $N = 11.28 \times 10^{22}$ per cm^3.

The author wishes to express his appreciation of the arrangement which made his participation in the CERN Theoretical Study Division in Copenhagen possible. It is a pleasure to thank Dr. Aage Bohr for enlightening discussions over section 3 and revision of the manuscript.

Appendix

The functions ${}_2F_1(l+r-n, l+2-n, 2l+2; -4n(n-1))$, with $r=1$ and 2, that appear in S_{nl} can be transformed in

$$(2n-1)^{n-l-r}\,{}_2F_1\left((l+n, l+r-n, 2l+2; \frac{4n(n-1)}{(2n-1)^2}\right)$$

by the usual relation

$${}_2F_1(a,b,c;x) = (1-x)^{-a}\,{}_2F_1\left(c-b, a, c; \frac{x}{x-1}\right).$$

In the case $n \gg l$, the new functions ${}_2F_1$ reduce, apart from the multiplicative term, to the type ${}_2F_1(\alpha+\lambda, \beta-\lambda, \gamma; x)$ where λ is large.

G. N. Watson [14]) investigated the asymptotic expansion of hypergeometric functions ${}_2F_1(\alpha+\varepsilon_1\lambda, \beta+\varepsilon_2\lambda, \gamma+\varepsilon_3\lambda; x)$ where λ is large compared to α, β, γ, and where ε_1, ε_2, ε_3 have the values $0, \pm 1$. The case we are dealing with is of the type $(1,-1,0)$. When using the notations of Watson, we define the quantities $x = \frac{1}{2}-\frac{1}{2}z$; $z = \cosh\ \zeta$; $\zeta = \xi+i\eta$ with the conventions $\xi \geqq 0$, $-\pi \leqq \eta \leqq \pi$. It is obvious that these conventions are unable to define uniquely ζ when x is real and $0<x<1$. Our case is of that type. In adding a fictitious imaginary part ϱ to z, the asymptotic expansion can be written without ambiguities, and the final expression is obtained by letting ϱ tend to 0. The first term of the asymptotic expansion, given in ref. [14]), p. 289, then becomes

$${}_2F_1(\alpha+\lambda, \beta-\lambda, \gamma; x) \approx \frac{\Gamma(\frac{1}{2})\Gamma(1-\beta+\lambda)\Gamma(\gamma)}{2\pi\Gamma(\gamma-\beta+\lambda)}$$

$$(\sin\eta/2)^{\frac{1}{2}-\gamma}(\cos\eta/2)^{\gamma-\alpha-\beta-\frac{1}{2}}\frac{\cos\left[\eta\left(\lambda+\frac{\alpha-\beta}{2}\right)+\frac{\pi}{2}(\frac{1}{2}-\gamma)\right]}{\lambda^{\frac{1}{2}}}$$

If we replace $\alpha, \beta, \gamma, \lambda$ and η by their values, the asymptotic value of the ratio

$$\frac{{}_2F_1(l+1-n, l+2-n, 2l+2; -4n(n-1))}{{}_2F_1(l+2-n, l+2-n, 2l+2; -4n(n-1))}$$

is

$$\frac{n-l-1}{n+l}\cot\left[\pi(n-l)-(5\pi/4+1)\right].$$

In using that result, the asymptotic expression of S_{nl} (7) contains no correction term linear in l/n.

References

1) M. G. E. Cosyns, C. C. Dilworth, G. P. S. Occhialini, M. Schoenberg, N. Page, Proc. Phys. Soc. A **62** (1949) 801; W. F. Fry, Phys. Rev. **79** (1950) 893; M.G.K. Menon, H. Muirhead, O. Rochat, Phil. Mag. **41** (1950) 583; A. Bonetti, G. Tomasini, Nuovo Cimento **8** (1951) 693
2) G. R. Burbidge, A. H. de Borde, Phys. Rev. **89** (1953) 189
3) A. H. de Borde, Proc. Phys. Soc. A **67** (1954) 57
4) M. B. Stearns, S. de Benedetti, M. Stearns, L. Leipuner, Phys. Rev. **93** (1954) 1123
5) M. Camac, M. L. Halbert, A. D. McGuire, J. B. Platt, Proceedings of the Glasgow Conference (1954) p. 288.
6) M. Camac, M. L. Halbert, J. B. Platt, Phys. Rev. **99** (1955) 905
7) M. H. Hebb, E. Nelson, Phys. Rev. **58** (1940) 486
8) B. Swirles, Proc. Roy. Soc. A **121** (1928) 447
9) W. Gordon, Ann. d. Phys. **2** (1929) 1031
10) W. Magnus, F. Oberhettinger, Formeln und Sätze für die speziellen Funktionen der Mathematischen Physik (1948) p. 13
11) F. G. Slack, Phys. Rev. **31** (1928) 527
L. R. Maxwell, Phys. Rev. **38** (1931) 1664
12) A. Kupper, Ann. d. Phys. **86** (1928) 511
13) W. Heitler, Quantum theory of radiation (1954) p. 207
14) G. N. Watson, Trans. Camb. Phil. Soc. **22** (1918) 277

Nuclear Physics, North-Holland Publishing Co., Amsterdam **1** (**1956**)

COLLOQUE DE PHYSIQUE NUCLEAIRE DE PARIS ET SACLAY (15-17 MARS 1956) †

Reçu le 23 avril 1956

Un Colloque organisé par la Section de Physique Corpusculaire de la Société Française de Physique s'est tenu à Paris et à Saclay les 15, 16 et 17 mars 1956. Cette réunion, consacrée à l'étude des modèles nucléaires, des réactions nucléaires et de la radioactivité, a réuni environ 180 participants parmi lesquels des représentants des laboratoires parisiens et des Universités de Strasbourg, Lyon, Grenoble, Bordeaux, Toulouse et Alger.

La première séance du Colloque s'ouvrit à 9 heures le jeudi 15 mars dans l'Amphithéâtre de Physique du Collège de France. Elle fut consacrée aux modèles nucléaires et aux réactions nucléaires.

Après l'allocution de bienvenue prononcée par M. le Professeur R. Lucas, Président de la Société Française de Physique, la séance débuta par un exposé de M. Claude Bloch (Physique Mathématique, Saclay = P.M.): mise au point sur le problème de la diffusion élastique dans la région de „moyenne énergie". Il parla de l'extension du modèle statistique de Thomas, Lane et Wigner à la diffusion inélastique et aux réactions, réactions photonucléaires en particulier. Cet exposé très clair constitua à la fois une excellente mise au point et un aperçu de vues originales sur la question.

M. Nataf (Physique et Chimie Nucléaires, Collège de France = P.C.N.) exposa ses résultats sur la discussion des fondements du modèle unifié de Bohr-Mottelson. M. Yoccoz (P.C.N.) exposa ensuite un traitement variationnel des mouvements collectifs nucléaires. Enfin, M. C. Marty (P.C.N.) termina cette série de courtes communications théoriques en traitant de l'influence de la déviation par rapport à la symétrie axiale sur les spectres de rotation nucléaires.

Cette première matinée se termina par quatre communications expérimentales sur des sujets divers. D'abord on entendit deux

† Rapport rédigé par un groupe de chercheurs du Service de Physique Nucléaire, C.E.N., Saclay.

exposés sur les réactions photonucléaires; l'un de M. R. Chastel (P.C.N.) qui a utilisé les deux raies gamma de $^{7}Li+p$ pour analyser le spectre de photoprotons du cuivre et comparé ses résultats aux prévisions du modèle statistique, l'autre de M. R. Basile (Institut du Radium = I.R.) et M. C. Schuhl (Physique Nucléaire, Saclay = P.N.) qui ont utilisé le rayonnement de freinage d'un bétatron pour l'étude de discontinuités dans les courbes d'activation de divers noyaux par réactions (γ, n). Puis M. Barloutaud (P.N.) exposa les travaux effectués avec MM. Riou (I.R.) et T. Grjebine (P.N.) sur l'excitation coulombienne des isotopes du mercure, travaux qui permettent de déterminer l'évolution des probabilités réduites de transition au voisinage de la couche à 126 neutrons.

Enfin, la dernière communication de H. Faraggi, J. Olkowsky, J. Beydon, M. Crut, R. Chaminade et A. Papineau (P.N.; Radioéléments, Saclay et I.R.) fut consacrée aux résultats de l'analyse détaillée des radioéléments formés par bombardement du cuivre par des ions d'azote, d'oxygène et de néon accélérés au cyclotron. Ces résultats montrent que, dans les réactions sur le cuivre, le processus de formation du noyau composé intervient notablement, mais que les rendements observés sont en désaccord avec la théorie statistique.

La séance de l'après-midi fut consacrée aux modèles nucléaires et à la radioactivité.

L'exposé d'introduction de Mme N. Marty (P.C.N.) rappela les bases du modèle de Bohr et Mottelson et les corrections qui y ont été apportées pour rendre compte des faits expérimentaux (notamment les énergies des états de rotation). Les transitions E1 ne sont pas expliquées par ce modèle; diverses interprétations sont proposées (Rasmussen, Nilsson).

Certains des résultats d'un travail de R. Ballini et R. Barloutaud (P.N.) sur les états excités de ^{159}Tb ne peuvent pas être interprétés par le modèle collectif sous sa forme actuelle.

T. Yuasa et M. Nahmias (P.C.N.) étudièrent divers éléments au voisinage de la couche 14, notamment ^{25}Al et ^{25}Na, afin de préciser certaines irrégularités au voisinage de cette couche.

Perez Y. Jorba (Ecole Normale Supérieure = E.N.S.) communiqua un travail effectué sur la distribution angulaire et la polarisation de γ émis par des noyaux orientés à basse température (application à ^{147}Nd et ^{141}Ge). R. Omnes (P.M.) fit part d'un travail théorique

sur la possibilité de déterminer le signe de l'interaction quadrupolaire dans ^{111}Cd par corrélation angulaire entre γ polarisés.

P. Lehmann et J. Miller (P.N.) exposèrent les résultats de nouvelles expériences sur les corrélations angulaires $\gamma-\gamma$ dans ^{111}In en coïncidence différée, qui montrent l'effet du réarrangement du cortège, consécutif à la capture électronique et la variation de la corrélation avec le retard différant suivant la nature du composé; In métal, $In(OH)_3$ et In_2O_3.

R. Bouchez, J. Tobailem, J. Robert, R. Muxart, R. Mellet, P. et R. Daudel (Institut Fourier, Grenoble et I.R.) remesurèrent la différence de période de ^7Be pour Be métallique et pour BeF_2 amorphe. Leurs derniers résultats sont en accord avec ceux de Segré.

J. Laberrigue, P. Radvanyi et M. Langevin (P.C.N.) ont corrigé la courbe donnant le rendement de fluorescence K en fonction de Z et ont ainsi modifié les valeurs anciennement admises pour divers rapports capture L/capture K; un net désaccord avec la théorie subsiste sur ce point dans divers cas (^{79}Kr, ^{71}Ge).

A. Michalowicz (I.R.) étudia le fond continu en coïncidence avec la raie K, dû au freinage interne associé à la capture; ses résultats sont en accord avec les travaux de Morrison et Schiff.

Ce fut ensuite la communication de J. F. Detoeuf et R. Moch (Physique Atomique et Moléculaire, Collège de France = P.A.M.). La limite inférieure de la vie moyenne de ^{116}Cd vis-à-vis d'une désintégration β double a été évaluée à 6×10^{16} ans. L'examen de l'ensemble des résultats sur la double émission β porte à conclure qu'il n'y a pas de neutrinos du type Majorana.

A l'aide d'émulsions photographiques, M. Ader (P.A.M.) a poursuivi son étude des particules rares de long parcours, émises par divers émetteurs α.

J. P. Adloff et M. Perey (Strasbourg) exposèrent une étude sur les dérivés du francium (AcK) effectuée avec des émulsions.

J. Bellicard et A. Moussa (Lyon) décrivirent un spectromètre sans fer, muni d'un compteur à fenêtre de 10 $\mu g/cm^2$, ayant une luminosité de 1 % et permettant de distinguer les raies différant de 2 ‰. L'alimentation est stabilisée à environ 10^{-4}. Des études de spectres de raies et de rétrodiffusion ont été effectuées avec cet appareil

H. Vartapetian présenta ensuite la communication de L. Dick, R. Foucher, N. Perrin et H. Vartapetian (I.R.) sur les coïncidences rapides avec sélection d'énergies par INa. Le présentateur décrivit

l'appareillage et les performances obtenues, ainsi que des mesures de périodes d'états excités (par exemple $(1.8\pm0.3)\times10^{-9}$s dans $UX_1 \rightarrow UX_2$).

Une communication de Perrin porta sur les mesures de coefficient de conversion par coïncidences γX et $\gamma\gamma$ (notamment dans ^{102}Rh) utilisant cet appareillage.

La matinée du 16 mars fut consacrée à la visite du C.E.N. de Saclay.

M. Jean (Bordeaux) commença la réunion de l'après midi du 16 mars par un exposé extrêmement intéressant sur les oscillations de surface des noyaux pairs. Les communications suivantes concernaient des travaux expérimentaux.

Les transitions gamma et les cascades correspondantes dans ^{20}Ne(d,p) ^{21}Ne ont été analysées en utilisant des détecteurs à scintillations IK et INa avec discrimination en énergie (MM. Gorodetzky, Muller et Port, Strasbourg). Le temps de résolution des coïncidences rapides est de $6 \cdot 10^{-9}$ s.

Les corrélations angulaires $\gamma-\gamma$ dans ^{13}C(p, γ) ^{14}N et les corrélations p$-\gamma$ dans ^{10}B (d,p) ^{11}B ont été étudiées (MM. Gorodetzky, Gallmann et Croissiaux, Strasbourg).

Des résultats très intéressants sur la corrélation positon-négaton des paires de matérialisation interne ont été présentés (MM. Gorodetzky, Armbruster et Chevallier, Strasbourg). Les cas suivants ont été étudiés: niveau de 3.09 MeV de ^{13}C, niveau 4.43 MeV de ^{12}C (transition E2). Une discrimination en énergie est utilisée en faisant la somme des impulsions des deux détecteurs. Dans le cas du niveau de ^{16}O à 6,06 MeV (O^+, émetteur de paires), les mêmes auteurs ont analysé la distribution en énergie des électrons de la paire pour différents angles positon-négaton.

Des réactions par tritons ont été observées en utilisant des émulsions nucléaires et un faisceau de tritons accélérés par le Van de Graaff de l'Ecole Polytechnique. La réaction ^{7}Li (t, α) ^{6}He a notamment été étudiée. Ces expériences continuent celles qui avaient été faites par l'observation de réactions par tritons à l'intérieur d'une émulsion nucléaire, expériences qui avaient déjà donné de beaux résultats (Mme Magnac-Valette et M. P. Cuër, Strasbourg). Les réactions ^{9}Be (d, α) ^{7}Li et ^{9}Be (d, t)^{8}Be ont été étudiées à l'aide des émulsions (MM. Jung et Cuër, Strasbourg). Des résultats concernant

les niveaux de ^{8}Be ont été présentés par MM. C. Bockelmann (M.I.T., U.S.A.) et A. Lévêque (P.N.) sur l'étude de ^{10}B (d, α)^{8}Be à l'aide de plaques exposées au spectrographe du Van de Graaff du M.I.T. Le spectre obtenu ne comporte pas les niveaux observés à Strasbourg.

L'interférence entre stripping et formation du noyau composé a été clairement démontrée par l'étude des distributions angulaires des protons de ^{16}O (d, p) ^{17}O*. Des courbes d'excitation très précises pour différents angles ont été présentées (Mme Roclawski-Conjeaud et M. Cotton, P.N.).

Les derniers résultats concernant la mesure du moment magnétique du second état excité de ^{19}F (197 keV) ($\mu = +3.3 \pm 0.4$ m. n.) ont été obtenus en perturbant la distribution angulaire des gammas émis dans ^{19}F (p, p') par un champ magnétique extérieur; la cible étant liquide, il n'y a pas de perturbation autre que celle imposée; les études ont été faites avec des liquides de viscosité variable (Lehmann, Lévêque, Fiehrer et Pick, P.N.).

Deux des premiers niveaux de ^{18}F ont été observés dans ^{18}O (p, n) ^{18}F par l'étude des seuils de neutrons lents et par la mesure de l'énergie des gammas correspondants (Naggiar, Roclawski-Conjeaud, Szteinsznaider et Thirion, P.N.).

MM. Bishop et Bizot (E.N.S. Paris) ont étudié les gamma de la réaction ^{9}Be+p pour des énergies de protons jusqu'à 500 keV. Distribution angulaire des gamma et corrélations angulaires entre gamma en cascade conduisent à des valeurs de spin des niveaux du noyau composé ^{10}B.

La séance du 17 mars au matin, présidée par M. J. Yvon fut consacrée à des communications de neutronique.

Ce fut d'abord la communication de M. Verlet (E.N.S.) sur l'interprétation des résonances géantes dans la diffusion élastique des neutrons par les noyaux. En tenant compte de la polarisation du noyau-cible par le neutron diffusé, on peut faire tomber la valeur du potentiel complexe déduit des interactions nucléon-nucléon de 23 MeV à 8 MeV (Voir Lane et Verlet, Phys. Rev. **100** (1955) 956).

La communication de M. Auclair (Neutronique Expérimentale, Saclay = N.E.) présentée par M. Jacob, fut relative à l'étude de la variation du nombre moyen de neutrons produits par la fission de ^{239}Pu. L'étude, au spectromètre à cristal, de la variation avec l'énergie des neutrons incidents, du nombre moyen de neutrons produits

par la fission de ^{239}Pu montre qu'entre le domaine thermique et 0.35 eV, il est constant à 1 % près. Une mesure à 8 eV redonne le même rapport à 2 % près.

M. Joly (N.E.) parla ensuite de la mesure de la section efficace de capture de ^{236}U pour un spectre de neutrons thermiques. La mesure absolue de l'activité β de ^{237}U formé dans une pile par réaction de ^{236}U (n, γ) ^{237}U permet le calcul de la section efficace moyenne de capture radiative de ^{236}U. La valeur obtenue pour la pile de Saclay est de 24 ± 7b. Une nouvelle mesure confirme cette valeur qui s'interprète en tenant compte de l'effet des neutrons en cours de ralentissement.

MM. Netter, Julien, Corge et Ballini (P.N.) exposèrent des résultats sur les sections efficaces de fission par les neutrons entre 1.5 et 3 MeV. Les mesures de Naggiar et Szteinsznaider présentées à Genève (n° 355) ont été prolongées pour la fission de ^{239}Pu et ^{233}U dans le domaine des neutrons de 1 à 3 MeV. La section efficace de fission de ^{239}Pu présente un maximum faiblement accentué vers 2.2 MeV et celle de ^{233}U diminue jusqu'à vers 2 MeV puis reste à peu près constante.

La communication de MM. J. Martelly et C. Robert (N.E.) fut consacrée à l'étude expérimentale de la phase de transition entre le ralentissement et l'équilibre thermique des neutrons. On a mesuré dans le graphite le terme d'âge τ entre l'énergie 1.45 eV et les sources thermiques. Une première méthode d'empoisonnement du graphite présentée à Genève sous le n° 358 avait donné $\tau = 43 \pm 10\ cm^2$. En interprétant la répartition expérimentale des neutrons thermiques dans un empilement de graphite pur, on obtient $\tau = 50 \pm 5\ cm^2$.

Le décès de Madame Irène Joliot-Curie, survenu le 17 mars, a amené à clore prématurément en signe de deuil les travaux de la Réunion à la demande des orateurs inscrits, traduisant leur émotion devant la perte immense subie par la Physique Nucléaire Française. Les sessions consacrées à l'interaction des rayonnements avec la matière et aux techniques expérimentales n'ont pas eu lieu. Les titres des communications annoncées étaient les suivants:

- Relation énergie-parcours des ions lourds dans les émulsions, par A. Papineau (P.N.).
- Etude par déviation magnétique du ralentissement des particules alpha, par J. Blandin-Vial (Aimant Permanent, Bellevue).
- Energie moyenne d'ionisation et défaut d'ionisation des particules

alpha dans les gaz, par M. Genin (Laboratoire de Physique des Rayons X, Paris).

– Etat des recherches concernant la diffusion des rayons γ par les noyaux par L. Goldzahl et P. Eberhard (P. A. M.).

– Etat de nos connaissances sur les scintillateurs, par J. Labeyrie (Constructions Electriques, Saclay = C.E.).

– Spectromètre à scintillations (INa) pour la mesure des coïncidences alpha-gamma; applications, par R. Foucher, L. Dick, N. Perrin et H. Vartapetian (I.R.).

– Calcul des courbes de résolution des systèmes de coïncidences utilisant des scintillateurs, par L. Dick, R. Foucher, N. Perrin et H. Vartapetian (I.R.).

– Etude à l'aide d'un photomultiplicateur des impulsions produites dans un compteur proportionnel lors de la multiplication électronique, par G. Charpak et G. A. Renard (P.C.N.).

– Adaptation aux irradiations gamma intenses des compteurs Geiger-Muller à parois de verre et graphitage externe, par D.Blanc (P.A.M.).

– Chambre d'ionisation à remplissage rapide, par J. Olkowsky, G. Valladas et L. Cohen (P.N.).

– Un sélecteur de temps de vol et un nouvel amplificateur 2 MHz, par H. Guillon (C.E.).

– Construction d'un spectromètre β du type solénoïdal; calcul de la forme des raies et comparaison avec les résultats expérimentaux, par L. Dick (I.R.).

– Sur un tube de 150 kV fonctionnant suivant la réaction T(d,n) ^{4}He en vue de l'étude de la diffusion inélastique des neutrons rapides de 14 MeV, par C. Magnan (P.A.M.).

– Améliorations récentes apportées au Van de Graaff de l'Ecole Polytechnique, par R. Barjon et Schmouker (Ecole Polytechnique, Paris).

– Problèmes de réglage et d'étalonnage d'un bétatron de 31 MeV, par G. Boulègue et P. Chanson (D.E.F.A. – Issy les Moulineaux).

– Un accélérateur linéaire d'électrons de 2.3 MeV, par Th. Frelot, R. Combe et M. Feix (P.A.M.).

– L'accélérateur linéaire du C.E.N. de Saclay, par E. Picard (C.E.).

BOOK REVIEWS

JACQUES ERRERA, *Chimie Physique Nucléaire Appliquée* (Masson et Cie, Paris, 1955. 226 pages. 2100 fr. frçs).

En deux cents pages ce livre traite de l'ensemble de la physique nucléaire et de ses applications. C'est dire qu'aucun des problèmes qui y sont traités n'y fait l'objet d'un développement approfondi et qu'il s'agit plutôt du premier examen rapide d'un vaste domaine. Aussi bien l'auteur lui-même, dans sa préface, nous dit qu'il s'agit seulement de fournir au lecteur une base suffisante pour permettre la lecture d'ouvrages plus spécialisés.

Dans une première partie sont exposées les propriétés générales des noyaux atomiques et les lois qui gouvernent les réactions nucléaires. Les caractères généraux de la fission et l'énumération des principaux types de réacteurs en constituent la conclusion.

La seconde partie débute avec un examen rapide des méthodes de détection des rayonnements et est essentiellement consacrée à l'examen des applications des radioéléments et des rayonnements à de nombreux problèmes de science pure ou appliquée, les problèmes biologiques et médicaux étant exclus.

L'ouvrage est bien présenté, facile à lire. Il donnera sans trop de peine au lecteur non spécialisé une „teinture" de physique nucléaire pure et appliquée. Il est à craindre toutefois que, malgré l'avertissement de l'auteur, le lecteur ne se laisse facilement influencer par le caractère élémentaire de l'exposé et s'imagine avoir étudié un domaine qu'il n'aura fait qu'effleurer.

A. Berthelot

COMMISSARIAT À L'ÉNERGIE ATOMIQUE, *La prospection de l'Uranium* (Masson et Cie, Paris, 1955. 62 pages. 450 fr. frçs).

Il s'agit d'un petit livre rédigé par les techniciens du Commissariat Français à l'Energie Atomique destiné à vulgariser les connaissances de base relatives aux méthodes de prospection de l'uranium.

Les données géologiques de base, la description des principaux minerais illustrée par de belles planches en couleur, celle des appareils portatifs de détection, complétées par des considérations sur les caractères essentiels des gisements d'uranium constituent un ensemble de renseignements qui permettront aux candidats prospecteurs de se mettre en chasse dans les meilleures conditions.

A. Berthelot

S. GLASSTONE, *Principles of Nuclear Reactor Engineering* (D. van Nostrand Co., New York. 1955. ix + 861 pages.)

Dr. Glasstone's new book on nuclear reactor engineering is most likely to become a standard text-book in this field. Written with his well-known pedagogical skill it is a new readable book in the long list of text-books from the author's hand.

The discussions on reactor theory found in his earlier *Elements of Nuclear Reactor Theory* (written together wih M. C. Edlund) have been abridged considerably. New chapters have been included, dealing with reactor instrumentation, chemical processing, reactor materials, shielding, and heat transfer. Short descriptions are given of typical research reactors.

Unfortunately, the new data on power reactors, etc. released at the Geneva Conference, 1955, have not been included.

J. Kjær

M. A. SCHULTZ, *Control of Nuclear Reactors and Power Plants* (McGraw-Hill Publishing Co, New York, Toronto, London, 1955. viii—313 pages, 52s. 6d.).

The book starts with a short chapter commenting upon the purpose and the philosophy of control and operational safety work. Chapter 2 and 3, deal with what might be called technical reactor kinetics. The neutron density is described as a function of the reactivity together with the various phenomena affecting the reactivity such as Xenon and Samarium poisoning, reactor temperatures, fuel depletion etc. Chapter 4 deals with automatic reactor control. The reactor as a heat producing machine is described from a power control viewpoint and the properties of the temperature and the Xenon internal feedback loops are discussed. After a discussion of the general requirements for an automatic control system, the chapter ends with a detailed description of the external control-rod loop including its principle of operation, transient response and how these things are affected by reactivity temperature coefficients.

Chapter 5 treats control rod mechanisms in operational principle and practical detail. Chapter 6 represents an inventory of the problem: nuclear power plant control taking into consideration both the properties of the reactor and the heat exchangers. After a general survey of the way in which the reactor temperature program effects the steam pressure and temperature there follows a detailed discussion of reactor and boiler temperature kinetics. The chapter ends with a general description of the control principle for various plant programs as f. ex. a constant steam pressure program and the necessary combination of feedback loops in order to effect that. Chapter 7 gives some details upon the special instrumentation necessary for neutron flux or density measurements in a reactor considering the requirements of working range, the influence of the γ-radiation and the temperature.

Chapters 8; 9; 10 constitue another cross-section of the problems met with in reactor plant control. Here the operational situations of start-up, power operation and shutdown are discussed in some detail together with the operational safety aspects in each of these situations.

The book ends with a chapter about analogue computing technique applied to reactor control problems.

It is the opinion of the reviewer that this book is a valuable aid to practical reactor control work. Even though, as stated in the author's preface, the book mainly describes the properties of pressurized water reactors with solid fuel elements, the general principles apply to other types of thermal reactors also and in one way the type mentioned is the most difficult to control due to its comparatively small amount of inherent safety. All the way through the book, the reactor is regarded simply as a technical piece of equipment with certain properties when subject to regulation or loading. It is discussed in a clear way how this component can be fitted into a power producing plant and how the plant can be run safely in a technically reasonable way. It is a good point to stress that the entire plant is concerned when control problems are under discussion and not only the reactor. This is especially the case where operational safety is concerned. It would on the other hand have been an advantage to have other types of reactors presented to a greater extent. The control schemes for the plant depend to a large extent upon the type of reactor; and a chapter covering the properties at large of f. ex. boiling heterogenous and homogenous reactors would have been a nice complement to this otherwise very useful book. These critical remarks also apply to the possible uses of a reactor; the author considers steam production for electricity generation only.

R. Vestergaard

ON SYMBOLS, UNITS AND NAMES

The Commission for Symbols, Units and Nomenclature of the International Union of Pure and Applied Physics has accomplished a meritorious work in compiling the various lists of symbols and recommendations (Document U.I.P. 6) which we reproduce in full on the following pages. It should be a matter of international co-operation, or more simply of courtesy, for every physicist to conform in his writings to these recommendations, which have been very carefully considered and embody sufficient flexibility to suit all reasonable idiosyncrasies.

With this Document the task of the Commission is by no means completed. There is even some urgency in fixing several points of nomenclature before needlessly illogical or barbarous expressions now prevailing have taken root too deeply. In the domain of nuclear physics, there are in particular those points which are enumerated in the *Note on Nomenclature* printed on p. 72 of this volume and on the cover of each issue of the journal. The sanction of the Commission in such matters would be most welcome, even though it too can take a false step occasionally. The case in point is the misshapen "nuclide", which the Commission has ill-advisedly taken under its aegis. My representations have elicited the disconcerting reply that, although it was felt that I was right in advocating *nucleide*, the Commission found it very difficult to introduce any change now, in view of the number of international organizations which had already expressed their assent; however, it would encourage me to call attention to the desirability of adopting the correct form. In other words, it asks me to take over what is in fact its rightful role, because it is apparently too overawed by its own decision to reverse it. In any case, this journal is entitled to foster the use of *nucleide* with a good conscience.

In two respects, it is felt that a somewhat greater flexibility should be allowed than is granted in the Commission's Document. The recommended notation for chemical elements, with the mass number as a *left* superscript (e.g. ^{14}N) is undoubtedly the best, but especially in nuclear physics the handier *right* superscript (N^{14}) should be tolerated; moreover, the right *sub*script place should be allowed to serve for the neutron number if required, no confusion being likely to arise in such cases (e.g. ${}_7N_6^{13}$).

The other point concerns the time unit symbols. It is customary among life-time specialists to use the symbol sec rather than s for second; this has the advantage of greater distinctness and ought to be allowed to remain. It would be nice to fix the other time symbols as well; we have adopted the series

sec (*or* s), min, h, d, y

for

second, minute, hour, day, year.

As an argument against a = *annus* for the latter it is sufficient to observe that nowadays English and not Latin is the universal scientific language.

Finally I might point out that it has been decided, with a heavy heart, to accept in *Nuclear Physics* the rather foolish "barn" as the name of a convenient unit for nuclear cross-sections (1 barn = 10^{-24} cm^2). In this connexion, one is also in need of a short name for the length 10^{-13} cm; having in mind the relation of this order of nuclear dimensions with the range of forces between nucleons, would the word "span" (symbol sp) perhaps† be appropriate?

L. R.

† I hope the fact that "span" sometimes denotes a distance of 9 inches will not be adduced as an objection!

INTERNATIONAL UNION OF
PURE AND APPLIED PHYSICS

—

S.U.N. COMMISSION

UNION INTERNATIONALE DE
PHYSIQUE PURE ET APPLIQUÉE

—

COMMISSION S.U.N.

SYMBOLS AND UNITS

SYMBOLES ET UNITÉS

Document U.I.P. 6
(1955)

Report published
with the financial support
of the UNESCO

Publication faite
avec l'appui financier
de l'UNESCO

I. GENERAL RECOMMENDATIONS;
RECOMMANDATIONS GÉNÉRALES

1. Physical quantities; *Grandeurs physiques* 543
2. Units; *Unités* 543
3. Mathematical operations; *Opérations mathématiques* 544
4. Chemical elements; *Éléments chimiques* 544

II. PHYSICAL QUANTITIES; *GRANDEURS PHYSIQUES*

1. Space and time; *Espace et temps* 545
2. Mechanics; *Mécanique* 546
3. Kinetic theory of gases; *Théorie cinétique des gaz* 547
4. Thermodynamics; *Thermodynamique* 548
5. Electricity; *Électricité* 549
6. Light; *Lumière* 550
7. Atomic physics; *Physique atomique* 551

III. MATHEMATICAL OPERATIONS AND SYMBOLS;
OPÉRATIONS ET SYMBOLES MATHÉMATIQUES

1. Analysis; *Analyse* 552
2. Vectors and tensors; *vecteurs et tenseurs* 553

IV. UNITS; *UNITÉS.*

1. Prefixes; *Préfixes* 554
2. CGS units; *Unités CGS* 554
3. MKSA units; *Unités MKSA* 555
4. Non-coherent units; *Unités non-cohérentes* . . . 555

REMARK ON RATIONALISATION;
REMARQUE SUR LA RATIONALISATION . . . 556

Remark:

This report, composed by the commission of Symbols, Units and Nomenclature of the I.U.P.A.P. has been approved by the General Assemblies of the Union of Physics, held in 1948, 1951 and 1954.

The recommendations on the use of symbols for units, for physical quantities and for mathematical constants and operations contained in this report are in general in agreement with important international recommendations, *viz:*

Remarque:

Ce rapport, composé par la commission des Symboles, Unités et Nomenclature de l'U.I.P.P.A., a été approuvé par les Assemblées Générales de l'Union de Physique, tenues en 1948, 1951 et 1954.

Les recommandations concernant l'usage des symboles pour les unités, les grandeurs physiques et pour les constantes et opérations mathématiques, contenues dans ce rapport s'accordent en général avec des recommandations importantes internationales, *viz:*

(1) International Standardising Organisation (I.S.O.) — Project ISO. TC 12.
(2) Conférence Générale des Poids et Mesures (9ème C.G. 1948; 10-ème C.G. 1954).
(3) Union Internationale de Chimie Pure et Appliquée (1947, 1949, 1951).
(4) International Electrotechnical Committee (Int. Letter Symbols Publ 27, 1953).

I. GENERAL PRINCIPLES AND RECOMMENDATIONS.
PRINCIPES ET RECOMMANDATIONS GÉNÉRAUX.

1. Physical quantities:

(1) Symbols for physical quantities should be printed in italic (cursive) type.

The symbol for a physical quantity („grandeur physique" *Fr;* „physical magnitude", *Am;* „physikalische Grösse", *G*) is equivalent to the product of the numerical value or measure, being a pure number, and a unit:

physical quantity = numerical value × unit.

(2) Abbreviations, i.e. shortened forms of names or expressions, should not be used in physical equations. In the text the abbreviations should be written in ordinary roman type (e.g.: pf for partition function, EMF for electromotive force, etc.).

1. Grandeurs physiques:

(1) Les symboles des grandeurs physiques seront imprimés en caractères italiques (cursives).

Le symbole d'une grandeur physique („physical quantity" *Angl;* „physical magnitude", *Am;* „physikalische Grösse" *All.*) est équivalent au produit de la valeur numérique (ou mesure), qui est un nombre pur, et d'une unité:

grandeur physique = valeur numéque × unité.

(2) Des abréviations, des noms ou des expressions abrégées, ne seront pas utilisées dans des équations physiques. Dans le texte, les abréviations seront écrites en caractères romains ordinaires (p.ex.: fp au lieu de fonction de partitions F.E.M. au lieu de force électromotrice, etc.).

2. Units.

(1) Symbols for units of physical quantities should be printed in roman (upright) type.

(2) Symbols for units should *not* be followed by a full stop.

(3) Symbols for units derived from proper names should start with a capital roman letter. All other units should be printed in lower case roman type.

(4) Symbols for prefixes should be printed in lower case roman type, with the single exception of the prefixes: M = mega, G = giga and T = tera.

(5) Symbols for units should *not* be written in plural (e.g. do *not* write: 7 watts, but: 7 watt or 7 W).

2. Unités.

(1) Les symboles des unités des grandeurs physiques seront imprimés en caractères romains (droits).

(2) Les symboles des unités ne seront *pas* suivis d'un point.

(3) Les symboles des unités dérivées de noms propres seront imprimés en commençant avec un caractère majuscule romain. Toutes les autres unités seront imprimées en caractères minuscules romains.

(4) Les symboles pour préfixes seront imprimés en caractères minuscules romains, excepté les préfixes: M = méga, G = giga et T = téra.

(5) Les symboles des unités ne seront *pas* écrits au pluriel (p.ex. n'écrivez *pas*: 7 watts, mais: 7 watt ou 7 W).

3. Mathematical operations and signs.

(1) Symbols for mathematical operations should be printed in roman (upright) type. (e.g.: sin *kx*, exp *at*, log *A*).

(2) Symbols for mathematical operations should *not* be followed by a full stop.

(3) Numbers should be printed in upright figures. A comma or point may be used only to separate the whole numbers from the decimals.

(4) To facilitate the reading of large numbers the figures may be grouped in groups of three but *no* comma or point should be used (e.g. 2 573,421 736).

4. Chemical elements.

(1) Symbols for chemical elements should be written in roman (upright) type and are not followed by a full stop (e.g. Ca, C, H, D, He).

(2) The attached numerals should have the following meaning:

mass number $^{14}N_2$
atomic number $_7$ atoms/molecule

The right superscript place is left for indicating, if required, a state of ionisation or nuclear excited states (e.g. Ca^{2+}, PO_4^{3-}). It may be of advantage to omit the atomic number when there is no special reasons for indicating it.

(3) A species of atoms identical as regards atomic number and mass-number should be indicated by the word *nuclide*. The name *isotopes* should be reserved for atoms with the same atomic number, whereas *isobars* are atoms having the same mass number.

3. Opérations mathématiques et signes.

(1) Les symboles des opérations mathématiques seront imprimés en caractères romains (droits). (p. ex.: sin *kx*, exp *at*, log *A*).

(2) Les symboles des opérations mathématiques ne seront *pas* suivis d'un point.

(3) Les nombres seront imprimés en chiffres droits. La virgule ou le point est utilisé seulement pour séparer les nombres entiers des nombres décimaux.

(4) Pour faciliter l'écriture, les grands nombres peuvent être partagés en tranches de trois chiffres mais ne doivent *pas* être séparés par des points ni par des virgules (p.ex. 2 573,421 736).

4. Éléments chimiques.

(1) Les symboles des éléments chimiques seront imprimés en caractères romains (droits) et ne sont pas suivis d'un point (p.ex. Ca, C, H, D, He).

(2) Les indices attachés aux symboles des éléments ont les sens suivants:

nombre de masse $^{14}N_2$
nombre atomique $_7$ atomes/molecule

L'indice en haut à droite est réservé pour indiquer l'état d'ionisation ou des états nucléaires excités (p.ex. Ca^{2+}, PO_4^{3-}). S'il n'y a pas de raisons spéciales pour indiquer le nombre atomique, il peut être préférable de le supprimer.

(3) Une espèce d'atomes identiques dans leur nombre atomique et nombre de masse sera désignée par le mot *nuclide*. Le nom *isotopes* sera réservé pour des atomes ayant le même nombre atomique, tandis que des *isobares* sont des atomes ayant le même nombre de masse.

II. SYMBOLS FOR PHYSICAL QUANTITIES
SYMBOLES DES GRANDEURS PHYSIQUES

Remark:

(1) Where several symbols are given for one quantity, and no special indication is made, they are on equal footing.

2) In general no special attention is paid to the name of the quantity.

Remarque:

(1) Lorsque plusieurs symboles sont indiqués pour une même grandeur sans indication spéciale, ces symboles sont admissibles au même titre.

(2) En général on n'a pas accordé une attention spéciale au nom de la grandeur.

1. Space, time; *Espace, temps.*

length; *longueur*	l	
breadth; *largeur*	b	
height; *hauteur*	h	
radius; *rayon*	r	
diameter; *diamètre*: $d = 2r$	d	
path; *parcours*: $L = \int ds$	L, s	
area; *surface*	A, S	
volume; *volume*	V, v	
plane angle; *angle plan*	$\alpha, \beta, \gamma, \theta, \vartheta, \varphi$	
solid angle; *angle solide*	ω, Ω	
wave length; *longueur d'onde*	λ	
wave number; *nombre d'onde*: $\sigma = 1/\lambda$	$\sigma, \tilde{\nu}$	*
circular —; — *circulaire*: $k = 2\pi/\lambda$	k	
time; *temps*	t	
period; *période*	T	
frequency; *fréquence*: $\nu = 1/T$	ν, f	**
pulsatance; *pulsation*: $\omega = 2\pi\nu$	ω	
velocity; *vitesse*: $v = ds/dt$	v	
angular velocity; — *angulaire*: $\omega = d\varphi/dt$	ω	
acceleration; *accélération*: $a = dv/dt$	a	
angular acceleration; — *angulaire*: $\alpha = d\omega/dt$	α	
gravitational —; — *de la pesanteur*	g	
standard — —; — — *normale*	g_n	
v/c	β	

---

* $\tilde{\nu}$ is exclusively used in molecular spectroscopy; $\tilde{\nu}$ *est utilisé exclusivement en spectroscopie moléculaire.*

** In physics; *en physique*: ν.

2. Mechanics; *Mécanique.*

mass; *masse*	m
density; *masse volumique*: $\varrho = m/V$	ϱ
reduced mass; *masse réduite*	μ
momentum; *moment*: $p = mv$	$\boldsymbol{p}, p$
moment of inertia; *moment d'inertie*: $I = \int r^2 dm$	I, J
force, *force*	$\boldsymbol{F}, F$
weight; *poids*	G, (W) *
force moment; *moment d'une force*	$\boldsymbol{M}, M$
pressure; *pression*	p
traction; *traction*	σ
shear stress; *tension de cisaillement*	τ
gravitational constant; *constante de la gravitation*: $F(r) = G\, m_1 m_2 / r^2$	G
modulus of elasticity, Youngs modulus; *module d'élasticité*: $\sigma = E\ \Delta l/l$	E
shear modulus; *module de torsion*: $\tau = G \operatorname{tg} \gamma$	G
compressibility; *compressibilité*: $\varkappa = -(1/V)\, dV/dp$	$\varkappa$
bulk modulus; *modue de compression*: $K = 1/\varkappa$	K
viscosity, *viscosité*	η
kinematic viscosity; — *cinématique*: $\nu = \eta/\varrho$	ν
friction coefficient; *coefficient de frottement*	f
surface tension; *tension superficielle*	γ, σ
energy, *énergie*	E, U
potential energy; *énergie potentielle*	V, E_p
kinetic energy; *énergie cinétique*	T, E_k
work; *travail*	W, A
power; *puissance*	P
efficiency; *rendement*	η
Hamiltonian function; *fonction de Hamilton*	H
Lagrangian function; *fonction de Lagrange*	L
relative density; *densité relative*	d

* Preferred symbol; *symbole préféré*: G.

3. Kinetic theory of gases; *Théorie cinétique des gaz.*

number of molecules; *nombre de molécules*	N
— per mole; — *par mole*	N_0, N
— per volume, number density; — *par volume*	n
mol. velocity vector with components; *vecteur de la vitesse moléculaire et ses composantes*	$\mathbf{c}$, (c_x, c_y, c_z) $\mathbf{u}$, (u_x, u_y, u_z)
mol. position vector with components; *vecteur de position moléculaire et ses composantes*	$\mathbf{r}$, (x, y, z)
mol. momentum vector with components; *vecteur du moment moléculaire et ses composantes*	$\mathbf{p}$, (p_x, p_y, p_z)
average velocity; *vitesse moyenne*	$c_0, u_0, \bar{c}, \bar{u},$
most probable speed; *vitesse la plus probable*	$\hat{c}, \hat{u}$
mean free path; *libre parcours moyen*	l
velocity distribution function; *fonction de distribution des vitesses*: $n = \int\int f\, du_x du_y du_z$	$f(c)$
Boltzmann's function; *fonction de Boltzmann*	H
generalized coordinate; *coordonnée généralisée*	q
generalized momentum; *moment généralisé*	p
volume in γ phase space; *volume dans l'espace* γ	Ω
thermodynamic temperature; *température thermodynamique*	T, (Θ) *
Boltzmann's constant; *constante de Boltzmann*	k
$1/kT$ in exponential functions; $1/kT$ *dans les fonctions exponentielles*	β
gas constant per mole; *constante molaire des gaz*	R
characteristic temperature; *température caractéristique*:	Θ
Debye —; — *de Debye*: $\Theta_D = h\nu_D/k$	Θ_D
Einstein —; — *d'Einstein*: $\Theta_E = h\nu_E/k$	Θ_E
rotational —; — *de rotation*: $\Theta_r = h^2/8\pi^2 Ik$	Θ_r
vibrational —; — *de vibration*: $\Theta_v = h\nu/k$	Θ_v

* Preferred symbol; *symbole préféré*: T.

4. Thermodynamics; *Thermodynamique*.

quantity of heat; *quantité de chaleur*	Q	
work; *travail*	W, A	
temperature; *température*	$t, (\vartheta)$	*
thermodynamic temperature; *température thermodynamique*	$T, (\Theta)$	**
entropy; *entropie*	S	
internal energy; *énergie interne*	U	
free energy, Helmholtz function; *énergie libre, fonction de Helmholtz*: $F = U - TS$	F	
enthalpy, heat function; *enthalpie*: $H = U + pV$	H	
Gibbs function; *enthalpie libre, fonction de Gibbs*: $G = U + pV - TS$	G	
linear expansion coefficient; *coefficient de dilatation linéaire*	a	
cubic expansion coefficient; *coefficient de dilatation cubique*	γ	
thermal conductivity; *conductibilité calorifique*	λ	
specific heat; *chaleur spécifique*	c_p, c_v	
molar heat capacity; *capacité thermique molaire*	C_p, C_v	
Joule-Thomson coefficient; *coefficient de Joule-Thomson*	μ	
ratio of specific heats; *rapport des chaleurs spécifiques*	$\varkappa, \gamma$	

* Preferred symbol; *symbole preferé: t.*
** Preferred symbol; *symbole préféré: T.*

5. Electricity; *Electricité.*

quantity of electricity, *quantité d'électricité*	Q
charge density; *densité électrique*	ϱ
surface charge density; — — *superficielle*	σ
electric potential; *potentiel électrique*	V
electric field; *champ électrique*	$\boldsymbol{E}, E$
electric displacement; *déplacement électrique*	$\boldsymbol{D}, D$
capacity; *capacité*	C
permittivity; *permittivité*: $\varepsilon = D/E$	ε
permittivity of vacuum; *permittivité du vide*	ε_0
relative permittivity; — *relative* $\varepsilon_r = \varepsilon/\varepsilon_0$	ε_r
dielectric polarization; *polarisation diélectrique*: $\boldsymbol{D} = \varepsilon_0 \boldsymbol{E} + \boldsymbol{P}$ †	$\boldsymbol{P}, P$
electric susceptibility; *susceptibilité électrique*:	χ_e
electric dipole moment, *moment dipolaire électrique*	$\mathbf{p}, p$
electric current; *courant électrique*	I
electric current density; *densité de* — —	$\boldsymbol{J}, J$
magnetic field; *champ magnétique*	$\boldsymbol{H}, H$
magnetic induction; *induction magnétique*	$\boldsymbol{B}, B$
magnetic flux; *flux magnétique*	Φ
permeability; *perméabilité*; $\mu = B/H$	μ
permeability of vacuum; *perméabilité du vide*	μ_0
relative permeability; — *relative*: $\mu_r = \mu/\mu_0$	μ_r
magnetization; *aimantation* $\boldsymbol{B} = \mu_0 (\boldsymbol{H} + \boldsymbol{M})$ †	$\boldsymbol{M}, M$
magnetic susceptibility; *susceptibilité magnétique*:	χ_m
electromagnetic moment; *moment électromagnétique*	$\boldsymbol{\mu}, \mu$
magnetic polarization; *polarisation magnétique*: $\mu_0 \boldsymbol{M}$	*
magnetic dipole moment; *moment magnétique dipolaire*	$\boldsymbol{m}, m$
resistance; *résistance*	R

† Written in the rational form. See page 556;
Écrite sous la forme rationalisée. Voir la page 556.

* No symbol is recommended; *pas de symbole recommandé.*

reactance; *réactance*	X
impedance; *impédance*: $Z = R + iX$	Z
conductance; *conductance:* $G = R/Z^2$	G
susceptance; *susceptance:* $B = -X/Z^2$	B
admittance; *admittance* $Y = 1/Z = G + iB$	Y
resistivity; *résistivité*	ϱ
conductivity; *conductivité* $1/\varrho$	γ, σ
self inductance; *inductance propre*	L
mutual inductance; *inductance mutuelle*	M, L_{12}
phase number; *nombre de phases*	m
loss angle; *angle de pertes*	δ
number of turns; *nombre de tours*	N
power; *puissance*	P
Poynting vector; *vecteur de Poynting*	$\mathbf{S}, S$
vector potential; *potentiel vecteur*	$\boldsymbol{A}$

6. Light; *Lumière.*

quantity of light; *quantité de lumière*	Q
flux of light; *flux de lumière*	Φ
luminous intensity; *intensité lumineuse*: $d\Phi/d\omega$	I
illumination; *éclairement*: $d\Phi/dS$	E
luminance; *luminance*: $dI/dS \cos\vartheta$	L, B
luminous radiance; *émittance lumineuse*: $d\Phi/dS$	H
absorption factor; *facteur d'absorption*: Φ_a/Φ_0	a
reflection factor; *facteur de réflexion*: Φ_r/Φ_0	ϱ
transmission factor; — *de transmission*: Φ_τ/Φ_0	τ
absorption coefficient; *coefficient d'absorption*	a
extinction coefficient; *coefficient d'extinction*	$\varkappa$
speed of light in empty space; *vitesse de la lumière dans le vide*	c
refractive index; *indice de réfraction*: $n = c/c_n$	n

7. Atomic and nuclear physics; *Physique atomique et nucléaire.*

atomic number; *nombre atomique*	Z
mass number; *nombre de masse*	A
proton number; *nombre de protons*: $P = Z$	P
neutron number; *nombre de neutrons*: $N = A - Z$	N
charge of electron; *charge électrique de l'électron*	$-e$
electron mass; *masse de l'électron*	m
proton mass; *masse du proton*	M_p
neutron mass; *masse du neutron*	M_n
meson mass; *masse du méson*	m_π, m_μ
nuclear mass; *masse nucléaire*	M
atomic mass; *masse atomique*	M_a
magnetic moment of particle; *moment magnétique d'une particule*	μ
magnetic moment of proton; — *du proton*	μ_p
magnetic moment of neutron; — *du neutron*	μ_n
magnetic moment of electron; — *électronique*	μ_e
Bohr magneton; *magnéton de Bohr*	μ_B, β
principal quantum number; *nombre quantique principal*	n, n_i
orbital angular momentum quantum number; *nombre quantique du moment angulaire*	L, l_i
spin quantum number; — — *du spin*	S, s_i
total angular momentum quantum number; *nombre quantique du moment total*	J, j_i
magnetic quantum number; — — *magnétique*	M, m_i
nuclear spin quantum number; — — *du spin nucléaire*	I
hyperfine quantum number; — — *hyperfin*	F
rotational quantum number; — — *de rotation*	J, K
vibrational quantum number; — — *de vibration*	v
quadrupole moment; *moment quadripolaire*	Q
Rydberg constant; *constante de Rydberg*	R

III. MATHEMATICAL OPERATIONS AND SYMBOLS
OPÉRATIONS ET SYMBOLES MATHÉMATIQUES

1. Analysis; *Analyse.*

equal to; *égal à*	$=$
approximately equal to; *égal environ à*	$\simeq, \approx$
proportional to; *proportionnel à*	$\propto$
tends to; *tend vers*	$\rightarrow$
asymptotically equal to; *asymptotiquement égal à*	$\sim$
corresponds to; *correspond à*	$\widehat{=}$
plus or minus; *plus ou moins*	$\pm$
sum of; *somme de*	Σ
product of; *produit de*	Π
infinity; *infini*	∞
pi; *pi*	π
base of natural logarithm; *base des logarithmes naturels*	e
factorial n; *factoriel* n	$n!$
binomial coefficient, *coefficient du binome:* $n!/p!(n-p)!$	$\binom{n}{p}$
variation of x; *variation de* x	δx
increase of x; *accroissement de* x	Δx *
exponential of x; *exponentielle de* x	$\exp x$, e^x
decadic log. of x; *log. décimal de* x	$\log x$ **
natural log. of x; *log. naturel de* x	$\ln x$
real part of z; *partie réelle de* z	$\mathrm{Re}\, z$
imaginary part of z; *partie imaginaire de* z	$\mathrm{Im}\, z$
modulus of z; *module de* z	$\lvert z \rvert$
complex conjugate of z; *conjuguée complexe de* z	z^*
complex conjugate of matrix A; *conjuguée complexe de la matrice* A: $(A^*)_{jk} = (A_{jk})^*$	A^*

---

* Greek capital delta, not triangle! *delta capitale grecque et non triangle!*

** In case of ambiguity ${}^{10}\log x$ or $\log_{10} x$; *en cas d'ambiguïté* ${}^{10}\log x$ ou $\log_{10} x$.

Hermitian conjugate of matrix A; *conjuguée Hermitienne de la matrice* A: $(A^\dagger)_{jk} = A_{kj}^*$ — $A^\dagger$

adjoint of matrix A; *adjoint de la matrice* A: $\tilde{A}_{jk} = A_{kj}$ — $\tilde{A}$

2. Vectors and tensors; *Vecteurs et tenseurs.*

To avoid the usage of subscripts it is often recommended to indicate vectors and tensors of the second rank by letters of a special type.

The following choice is recommended:

(1) *Vectors should be printed in bold type by preference bold italic type.*

(2) *Tensors of the second rank should be printed in sans serif type.*

(3) In manuscripts vectors may be indicated by an arrow and tensors by a double arrow on top.

Pour éviter l'usage d'indices il est souvent recommandé d'indiquer les vecteurs et les tenseurs du second ordre par des caractères spéciaux.

Le choix suivant est recommendé:

(1) *Les vecteurs seront imprimés en caractères gras, de préférence aux caractères italiques.*

(2) *Les tenseurs du second ordre seront imprimés en caractères sans sérif.*

(3) Dans les manuscrits les vecteurs peuvent être indiqués par une flèche et les tenseurs par deux flèches surmontant la lettre.

---

vector; *vecteur*	$\boldsymbol{A}$, $\boldsymbol{a}$
absolute value; *valeur absolue*	$\lvert\boldsymbol{A}\rvert$, $\lvert\boldsymbol{a}\rvert$
scalar product; *produit scalaire*	$\boldsymbol{A}\cdot\boldsymbol{B}$
vector product; *produit vectoriel*	$\boldsymbol{A}\wedge\boldsymbol{B}$, $\boldsymbol{A}\times\boldsymbol{B}$
nabla operator, *opérateur nabla*	∇
gradient; *gradient*	grad φ, $\nabla\varphi$
divergence; *divergence*	div $\boldsymbol{A}$
curl; *rotationnel*	curl $\boldsymbol{A}$, rot $\boldsymbol{A}$
Laplacian; *Laplacien*	$\Delta\varphi$, $\nabla^2\varphi$
dyadic product; *produit dyadique*	$\boldsymbol{A}\,\boldsymbol{B}$
tensor; *tenseur*	T
tensor product; *produit tensoriel*: $\Sigma_k S_{ik} T_{kl}$	$\mathsf{S}\cdot\mathsf{T}$
scalar product; *produit scalaire*: $\Sigma_k\Sigma_i S_{ik} T_{ki}$	$\mathsf{S}:\mathsf{T}$
product of vector and tensor; *produit d'un vecteur et d'un tenseur* $\Sigma_k A_k T_{ki}$; $\Sigma_i T_{ki} A_i$	$\boldsymbol{A}\cdot\mathsf{T}$; $\mathsf{T}\cdot\boldsymbol{A}$

IV. SYMBOLS FOR UNITS.
SYMBOLES DES UNITÉS.

1. Symbols for prefixes; *Symboles des préfixes.*

deci; *déci*	$(= 10^{-1})$	d	kilo; *kilo*	$(= 10^{3})$	k
centi; *centi*	$(= 10^{-2})$	c	mega; *méga*	$(= 10^{6})$	M
milli; *milli*	$(= 10^{-3})$	m	giga; *giga*	$(= 10^{9})$	G
micro; *micro*	$(= 10^{-6})$	μ	tera; *téra*	$(= 10^{12})$	T
nano; *nano*	$(= 10^{-9})$	n			
pico; *pico*	$(= 10^{-12})$	p			

2. CGS-Units; *Unités CGS.*

	Unit; *Unité*	Symbol; *Symbole*
l, b, h	centimeter; *centimètre*	cm
t	second; *seconde*	s
m	gram; *gramme*	g
f, ν	hertz; *hertz* $(= s^{-1})$	Hz
F	dyne; *dyne*	dyn
E	erg; *erg*	erg
p	barye; *barye* $(= \text{dyn/cm}^2)$	barye
η	poise; *poise* $(= \text{dyn s/cm}^2)$	P
T	degree Kelvin; *degré Kelvin*	°K
t	degree Celsius; *degré Celsius*	°C
H	oersted; *oersted*	Oe
B	gauss; *gauss*	G
Φ	maxwell; *maxwell*	Mx
F_M	gilbert; *gilbert*	Gi
I	candela; *candéla*	cd
Φ	lumen; *lumen* $(= \text{cd.sr})$	lm
L, B	stilb; *stilb* $(= \text{cd/cm}^2)$	sb
E	phot; *phot* $(= \text{lm/cm}^2)$	phot
α	radian; *radian*	rad
ω	steradian; *stéradian*	sr

3. MKSA-Units; *Unités MKSA.*

	Unit; *Unité*	Symbol; *Symbole*
l, b, h	meter; *mètre*	m
t	second; *seconde*	s
m	kilogram; *kilogramme*	kg
ν, f, ω	hertz; *hertz*	Hz
F	newton; *newton*	N
E	joule; *joule*	J
P	watt; *watt*	W
I	ampere; *ampère*	A
Q	coulomb; *coulomb*	C
V	volt; *volt*	V
C	farad; *farad*	F
R	ohm; *ohm*	Ω
L	henry; *henry*	H
Φ	weber; *weber*	Wb
I	candela; *candéla*	cd
Φ	lumen; *lumen*	lm
L, B	nit; *nit* (= cd/m^2)	nt
E	lux; *lux* (= lm/m^2)	lx

4. Non-coherent Units; *Unités non-cohérentes.*

	Units; *Unités*	Symbol; *Symbole*
l	ångström; *ångström*	Å
V	liter; *litre*	l
t	minute; *minute*	min
t	hour; *heure*	h
p	atmosphere; *atmosphère*	atm
P	kilowatt-hour; *kilowatt-heure*	kWh
Q	calorie; *calorie*	cal
Q	kilocalorie; *kilocalorie*	kcal
m	tonne; *tonne* (= 1000 kg)	t
p	bar; *bar* ($=10^5$ barye)	bar

Remark on rationalisation

(1) In 1951 the I.U.P.A.P. accepted the following *resolution:*

„The General Assembly of the Union of Physics considers that, in the case that the equations are rationalised, the rationalisation should be effected by the introduction of new quantities."

(2) When confusion is possible between rational and non-rational quantities it is recommended to add to the name of the quantity the adjective „*rational*" or „*non-rational*" and to provide the symbol of the quantity with a left subscript n or r respectively. E.g.:

non-rational magnetic field $= {}_{\mathrm{n}}H$,
rational magnetic field $= {}_{\mathrm{r}}H$,
${}_{\mathrm{r}}D = {}_{\mathrm{n}}D/4\pi$ but ${}_{\mathrm{n}}E = {}_{\mathrm{r}}E = E$,
${}_{\mathrm{r}}H = {}_{\mathrm{n}}H/4\pi$ but ${}_{\mathrm{n}}B = {}_{\mathrm{r}}B = B$,

(3) In order to transform an equation between non-rational quantities into an equation between rational quantities, the following table gives the rational quantities and the equivalent expressions in terms of the non-rational quantities:

Remarque sur la rationalisation

(1) En 1951 l'U.I.P.P.A. à adopté la *résolution* suivante:

„L'Assemblée Générale de l'Union de Physique considère que, dans le cas où les équations sont rationalisées, la rationalisation doit être obtenue par l'introduction de grandeurs nouvelles."

(2) Quand il y a une possibilité de confusion entre grandeurs rationnelles et non-rationnelles il est recommandé d'ajouter l'adjective „*rationnel*" ou „*non-rationnel*" et de munir le symbole de la grandeur d'un indice en bas à gauche n ou r respectivement. P.ex.:

champ magnétique non-rationnel $= {}_{\mathrm{n}}H$
champ magnétique rationnel $= {}_{\mathrm{r}}H$
${}_{\mathrm{r}}D = {}_{\mathrm{n}}D/4\pi$ mais ${}_{\mathrm{n}}E = {}_{\mathrm{r}}E = E$
${}_{\mathrm{r}}H = {}_{\mathrm{n}}H/4\pi$ mais ${}_{\mathrm{n}}B = {}_{\mathrm{r}}B = B$

(3) Afin de transformer une équation entre grandeurs rationnelles en une équation entre grandeurs non-rationnelles, le tableau suivant donne les grandeurs rationnelles et les expressions équivalentes exprimées en grandeurs non-rationnelles:

rat.	non-rat.	rat.	non-rat.
Q	Q	I	I
ρ	ρ	J	J
E	E	B	B
D	$D/4\pi$	H	$H/4\pi$
P	P	M	M
ϵ	$\epsilon/4\pi$	μ	$4\pi\mu$
ϵ_0	$\epsilon_0/4\pi$	μ_0	$4\pi\mu_0$
ϵ_r	ϵ_r	μ_r	μ_r

(4) *Example:*
The horizontal component of the magnetic induction of the earth's magnetic field is in Europe approximately

$$B = 0{,}2\ \mathrm{G} = 0{,}2 \times 10^{-4}\ \mathrm{Wb/m^2}$$

This value *is unaffected by rationalisation.*

The corresponding non-rational magnetic field is:

$${}_{\mathrm{n}}H = 0{,}2\ \mathrm{Oe} = 0{,}2 \times 10^3\ \mathrm{A/m}$$

and the corresponding rational magnetic field is:

$${}_{\mathrm{r}}H = (0{,}2/4\pi)\ \mathrm{Oe} = (0{,}2 \times 10^3/4\pi)\ \mathrm{A/m} = 15{,}9\ \mathrm{A/m}$$

As the numerical value of the magnetic field *is affected by rationalisation,* it is advisable to use when possible the magnetic induction expressed in gauss or in $\mathrm{Wb/m^2}$.

(4) *Exemple:*
La composante horizontale de l'induction magnétique du champ magnétique terrestre en Europe est approximativement:

$$B = 0{,}2\ \mathrm{G} = 0{,}2 \times 10^{-4}\ \mathrm{Wb/m^2}$$

Cette valeur *ne dépend pas de la rationalisation.*

L'intensité du champ magnétique non-rationnel correspondant est

$${}_{\mathrm{n}}H = 0{,}2\ \mathrm{Oe} = 0{,}2 \times 10^3\ \mathrm{A/m}$$

et l'intensité du champ magnétique rationnel correspondant est:

$${}_{\mathrm{r}}H = (0{,}2/4\pi)\ \mathrm{Oe} = (0{,}2 \times 10^3/4\pi)\ \mathrm{A/m} = 15{,}9\ \mathrm{A/m}$$

Parceque la valeur numérique de l'intensité du champ magnétique *dépend de la rationalisation,* il est recommandable d'utiliser si possible l'induction magnétique exprimée en gauss ou en $\mathrm{Wb/m^2}$.

FOR PROSPECTIVE CONTRIBUTORS

Since the nomenclature in the field of Nuclear Physics is not yet quite unified and a number of illogical expressions are unfortunately still widely used, it is advisable to give the following indications about the terminology adopted in this journal.

(1) The word 'electron' applies to particles with an elementary charge of either sign. When it is desirable to emphasize the sign of the charge, the words 'positon' and 'negaton' are used. Thus the illogical phrase 'electron-positron pair' is replaced by 'electron pair', or, if required, by 'positon-negaton pair'.

(2) Nuclei (or nucleids, *not* 'nuclids') are conveniently divided according to the parity of the proton and neutron numbers Z, N, into four families as follows:

even mass nuclei	{ even nuclei (Z even, N even) odd nuclei (Z odd, N odd)
odd mass nuclei	{ odd proton nuclei (Z odd, N even) odd neutron nuclei (Z even, N odd).

(3) The expressions 'isotopic spin', 'isotopic quantum number' are replaced by 'isobaric spin', 'isobaric quantum number'.

(4) For the elementary particles use is made of the latest nomenclature adopted by international agreement.

Editors and publishers have taken steps to secure prompt publication of accepted contributions; to achieve this end they count on the co-operation of authors, who are expected, as a matter of course, to submit neatly prepared typescripts of well-written papers and to return carefully corrected proofs without delay.

Just out

QUANTUM FIELD THEORY

BY HIROOMI UMEZAWA

Professor in Theoretical Physics, Tokyo

The aim of this book is to present comprehensive treatises about relativistic field equations, their quantisation, renormalisation theory, scattering problems, methods of calculations and various specialized problems of known particles and their interactions.

1956 – 6 × 9 – XVI + 350 pages – f 35,– $ 9.25 £ 3.10.0

Sole Agency for U.S.A.:
INTERSCIENCE PUBLISHERS, INC. 250 Fifth Avenue, New York 1, N. Y.

NORTH-HOLLAND PUBLISHING COMPANY

STARTING
PUBLICATION IN FALL 1956

Pre-Announcement

NUCLEAR INSTRUMENTS

A journal on accelerators, instrumentation and techniques in nuclear physics

Editor: KAI SIEGBAHN, University of Uppsala, Sweden

NUCLEAR INSTRUMENTS will publish experimental, theoretical and technical articles on subjects like: accelerators, isotope separators and mass spectrometers, instruments for nuclear spectroscopy, counters and detectors of nuclear radiation, electronic equipment used for nuclear instrumentation and automation, miscellaneous nuclear techniques like the preparation of targets or high specific activity sources, magnetic field measurements and vacuum technique with particular bearing upon nuclear apparatus etc. Furthermore, articles will be accepted dealing with dosimetry, and with the instruments used in tracer technique. Survey articles, letters to the editor, short laboratory notes and book reviews will also be included.

NUCLEAR INSTRUMENTS is strictly international in character. The Editorial Board consists of nuclear physicists representing all countries active in this field.

Details of publication will be announced later.

NORTH-HOLLAND PUBLISHING COMPANY